METHODS FOR STRENGTHENING REINFORCED CONCRETE BRIDGE GIRDERS CONTAINING POORLY DETAILED FLEXURAL STEEL USING NEAR-SURFACE MOUNTED METALLICS

Final Report Appendices B-D

SPR 750

Oregon Department of Transportation

APPENDIX B

EXPERIMENTAL DATA FOR T SPECIMENS

APPENDIX B – EXPERIMENTAL DATA FOR T SPECIMENS

Appendix B describes the internal and external configuration of sensors to monitor data for each T-specimen. Illustrations are included for the diagonal displacement sensors and strain gage configuration. Data for all sensors was sampled at a rate of 5 Hz.

Support Settlement: Support settlements were measured with two 2 in. (50.8 mm) displacement sensors placed on each side of the web. Each sensor was labeled with "North-East," "North-West," "South-East," or "South-West." The sensors measured the settlement of the specimen at the support with reference to the ground. The sensor pairs were averaged to equate the total support settlement.

Midspan Displacement: Midspan displacement was measured using two 10 in. (254 mm) long string potentiometers mechanically attached to each side of the web at midspan. The displacements on the East and West side of the web were averaged for account for any rotation while testing. The average midspan displacement subtracted the support settlement to obtain the true midspan displacement.

Cutoff Bar Slip: Cutoff bar slip was measured characterize anchorage response with two 1 in. (25.4 mm) displacement sensors. The displacement sensors were attached using methods discussed in *Chapter 3 Instrumentation.* Both east and west cutoff bar slip was measured.

Diagonal Displacement Sensors: Diagonal displacement sensors were used to measure the change in crack widths crossing the sensor. The diagonal displacement sensors were mechanically attached to the stem of the specimens. Brass wire was strung from the diagonal displacement sensor to an opposing point. Two diagonal displacement sensors were placed over a specified length to measure compression and tension in the section. The sensors were numbered and installed according to Figure B.1 and Figure B.2 with the arrow indicating the direction of measurement.

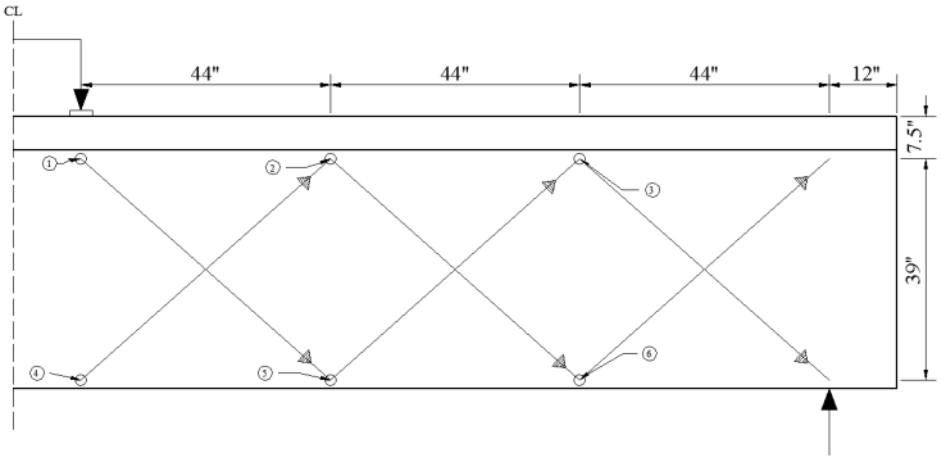

Figure B.1 Diagonal displacement sensor numbering on North side of specimen T.45.Ld3(10).Ti, T.45.Ld3(6).Ti andT.45.Ld3(6).SS

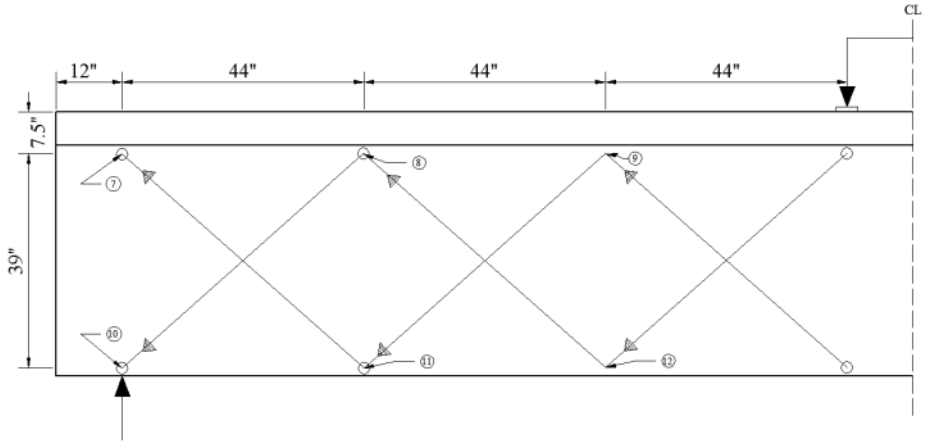

Figure B.2 Diagonal displacement sensor numbering on South side of specimen T.45.Ld3(6).Ti andT.45.Ld3(6).SS

Strain Gages: Stain gages were adhered to longitudinal reinforcing steel, NSM materials, and stirrups legs. Along the longitudinal reinforcing steel and NSM materials strain gages were located at the termination of the NSM material and the termination of the cutoff steel reinforcing bar. Stirrup strain gages were implemented on one leg along the preformed diagonal crack and at mid-height. The labeling convention of the strain gages can be found in Figure B.3 through Figure B.5. The strain gage location on the stainless steel NSM is coincident with the titanium on the top and bottom bars (bars 1 and 4). However, the label number for the stainless steel NSM materials are opposite of the titanium NSM material. A cross section is provided in Figure B.6 for the NSM titanium and stainless steel internal sensor configuration.

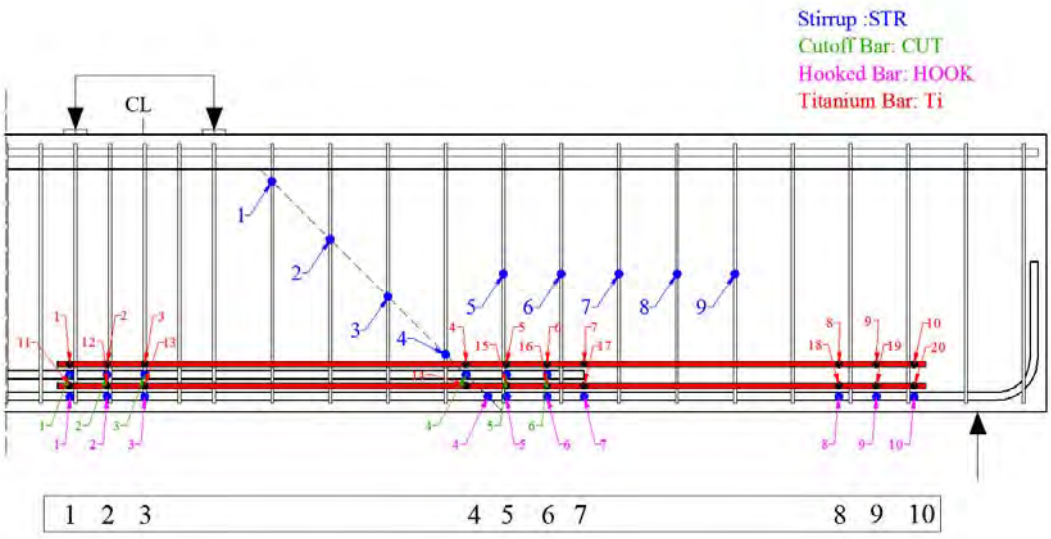

Figure B.3 - Specimen T.45.Ld3(10).Ti Strain gage labeling convention

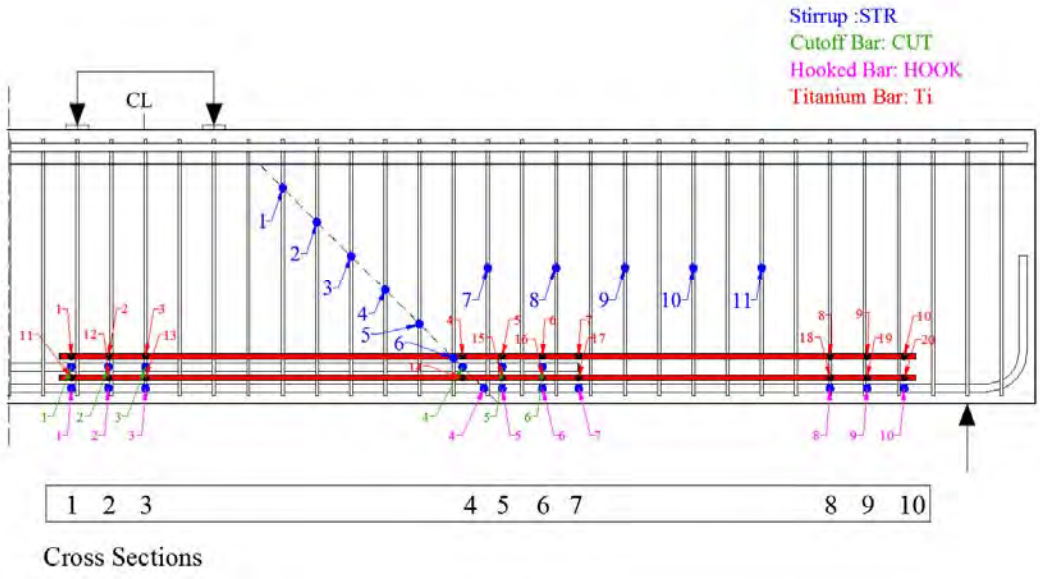

Figure B.4 - Specimen T.45.Ld3(6).Ti Strain gage labeling convention

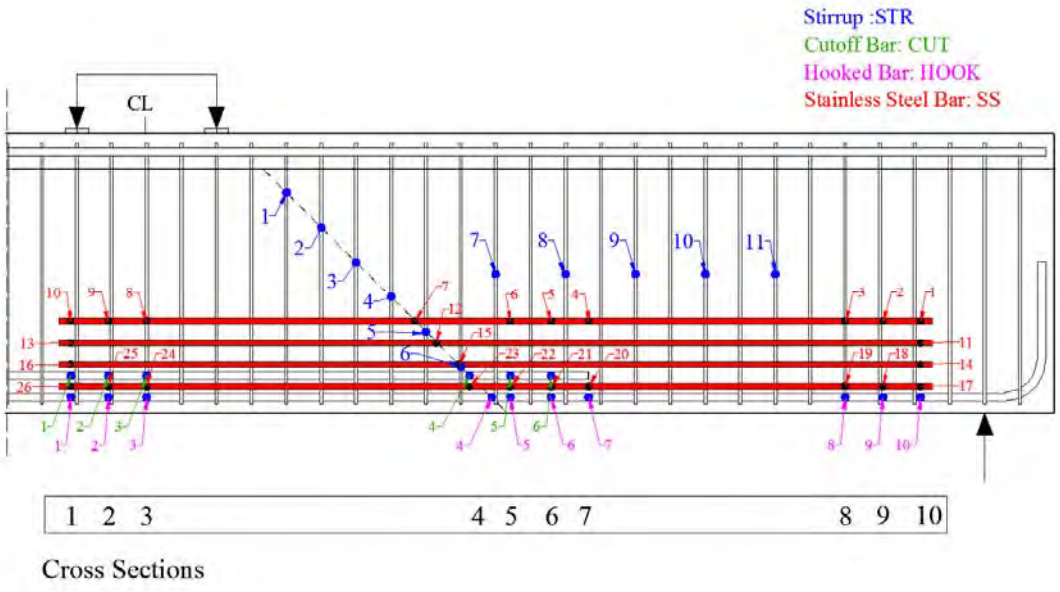

Figure B.5 - Specimen T.45.Ld3(6).SS Strain gage labeling convention

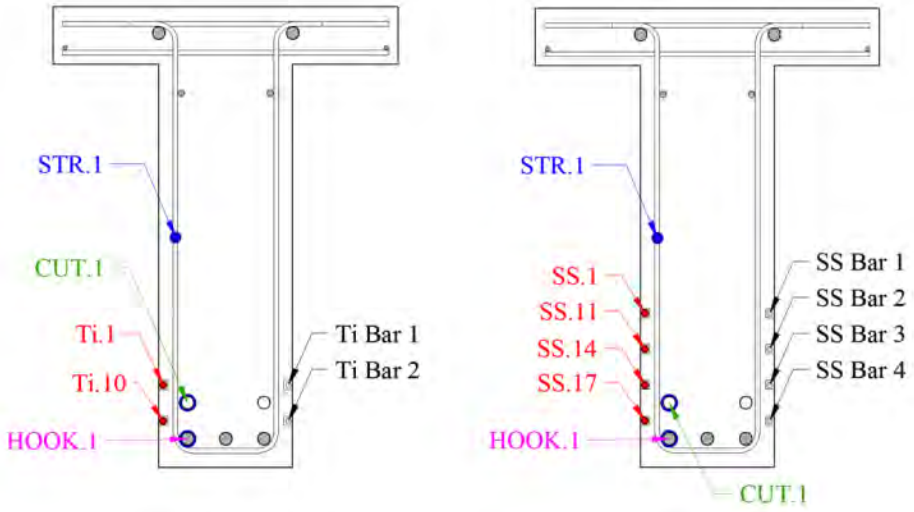

Figure B.6 - Cross section for internal instrumentation for T.45.Ld3(10).Ti and T.45.Ld3(6).Ti (left) and T.45.Ld3(6).SS (right)

B.1 T.45.Ld3(10).Ti

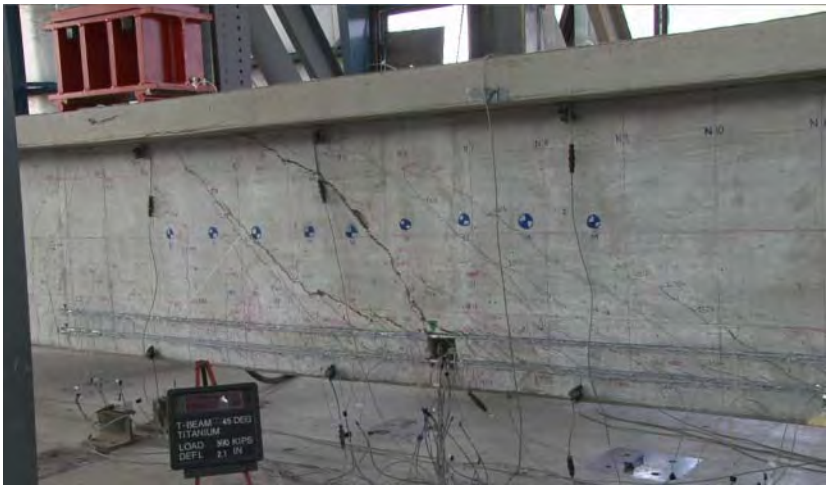

Figure B.7 - Specimen T.45.Ld3(10).Ti at failure

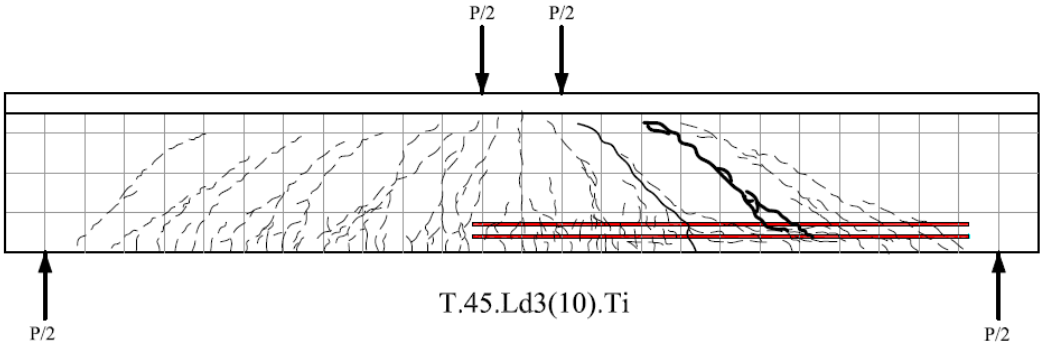

Figure B.8 - Specimen T.45.Ld3(10).Ti crack map

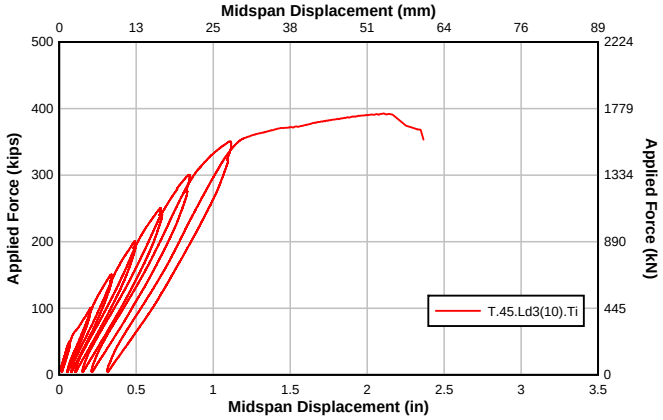

Figure B.9 - Specimen T.45.Ld3(10).Ti Load displacement curve

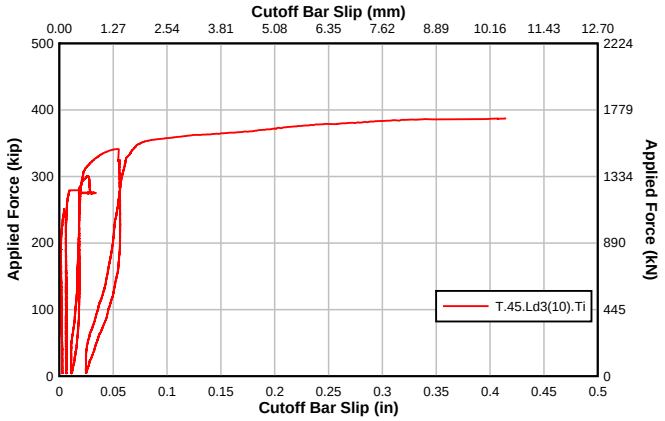

Figure B.10 - T.45.Ld3(10).Ti Cutoff bar slip

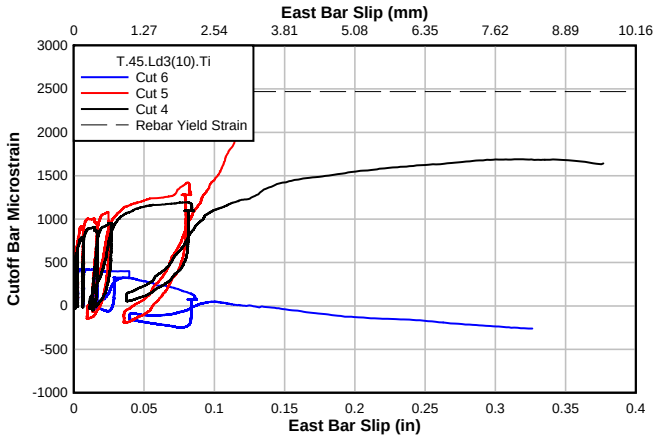

Figure B.11 - T.45.Ld3(10).Ti Slip and cutoff bar strain

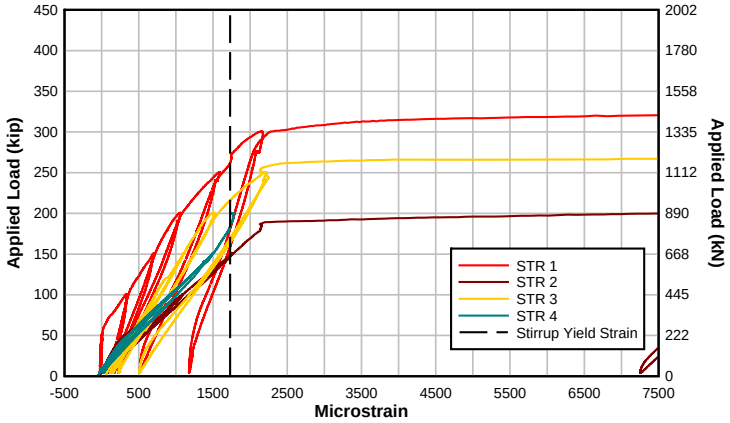

Figure B.12 - T.45.Ld3(10).Ti Strain in stirrups along diagonal crack

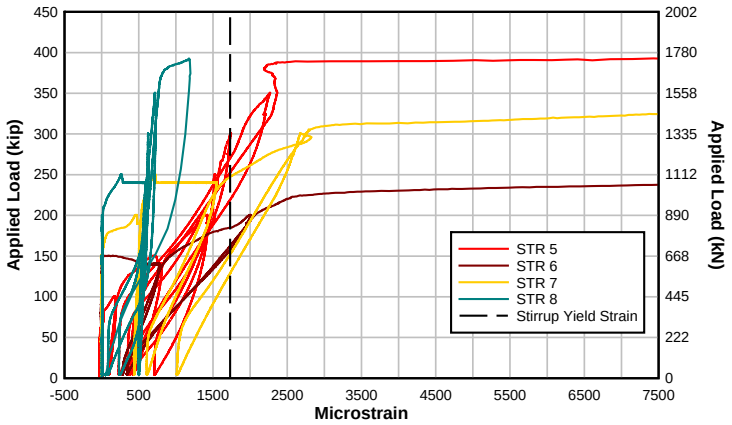

Figure B.13 - T.45.Ld3(10).Ti Strain in stirrups mid height

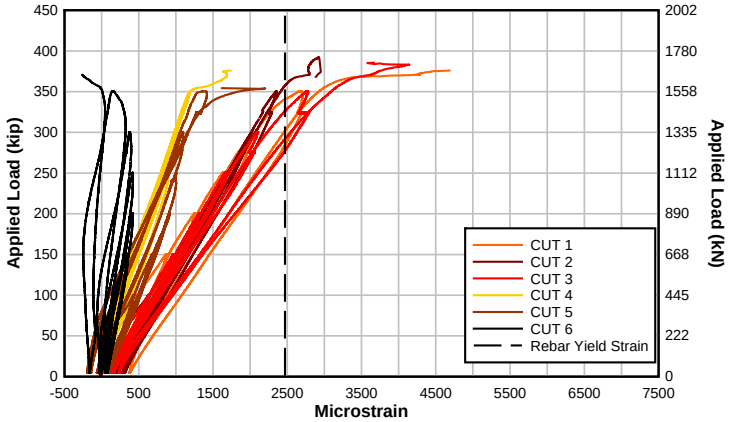

Figure B.14 - T.45.Ld3(10).Ti Strain in cutoff bar

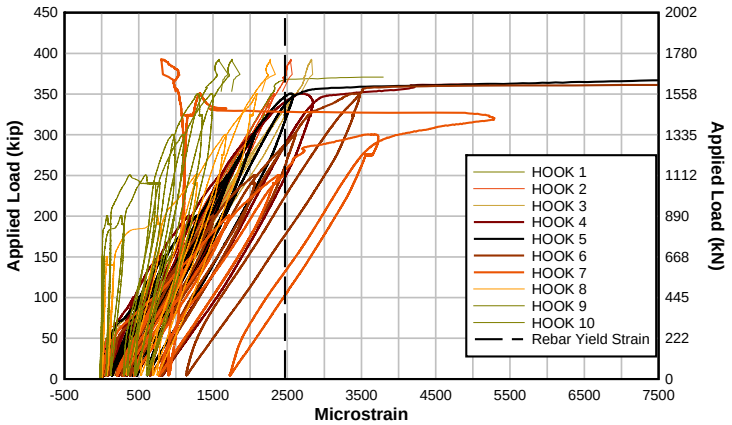

Figure B.15 - T.45.Ld3(10).Ti Strain in hook bar

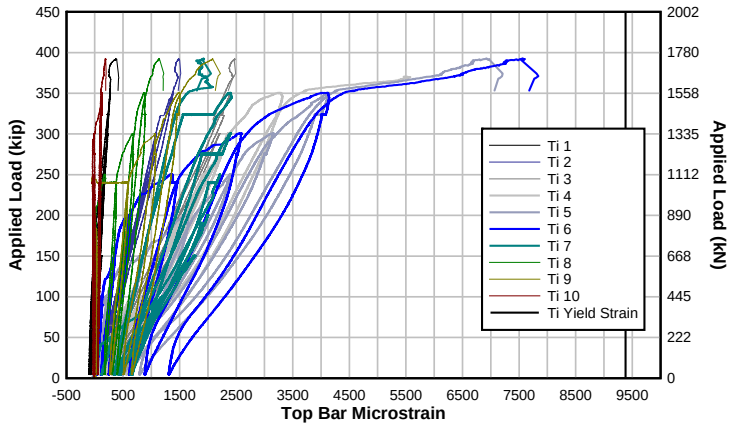

Figure B.16 - T.45.Ld3(10).Ti Strain in upper titanium bar

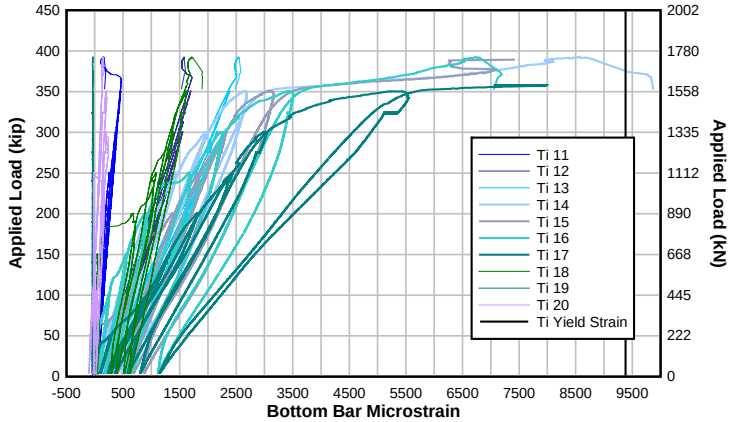

Figure B.17 - T.45.Ld3(10).Ti Strain in lower titanium bar

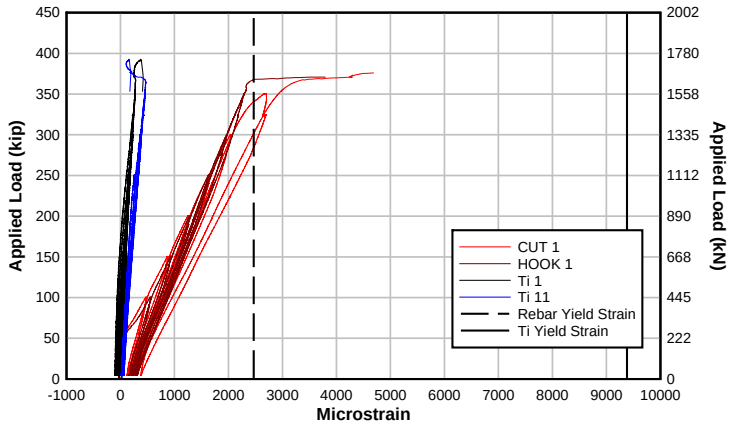

Figure B.18 - T.45.Ld3(10).Ti Section 1 strain

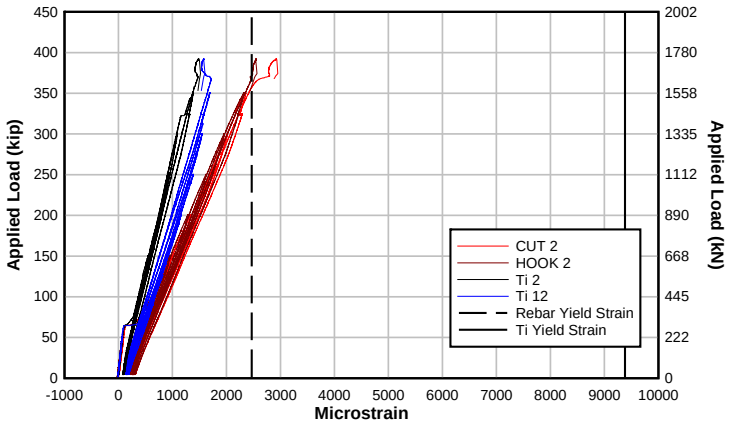

Figure B.19 - T.45.Ld3(10).Ti Section 2 strain

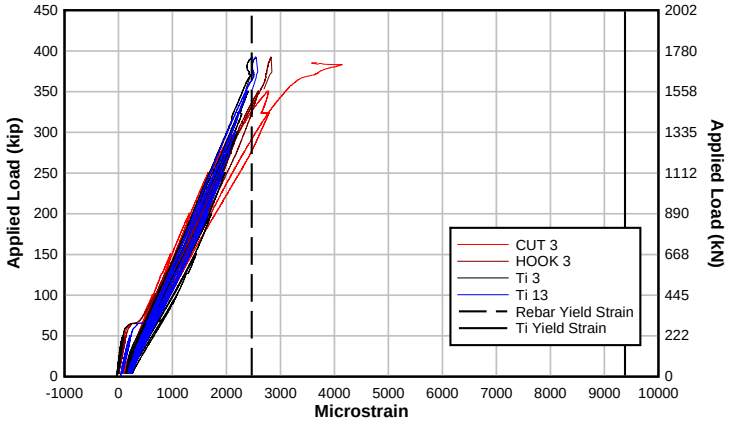

Figure B.20 - T.45.Ld3(10).Ti Section 3 strain

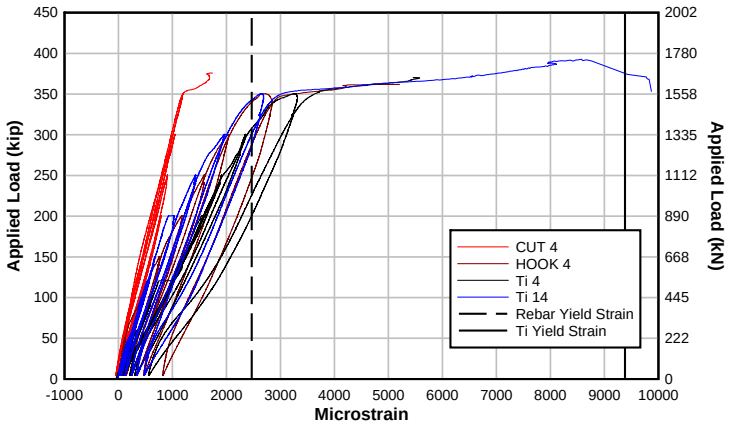

Figure B.21 - T.45.Ld3(10).Ti Section 4 strain

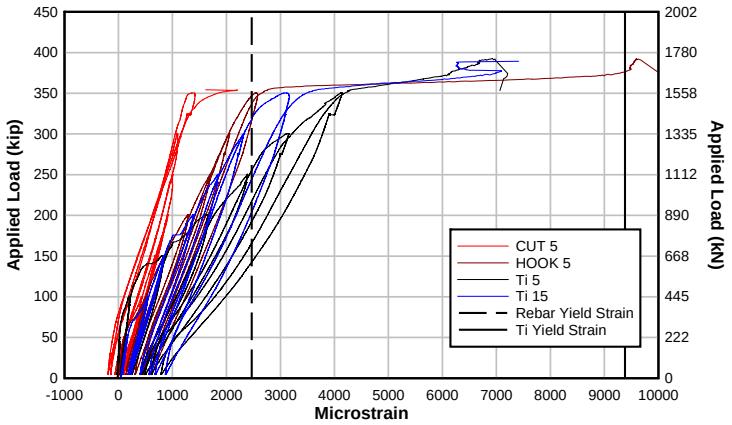

Figure B.22 - T.45.Ld3(10).Ti Section 5 strain

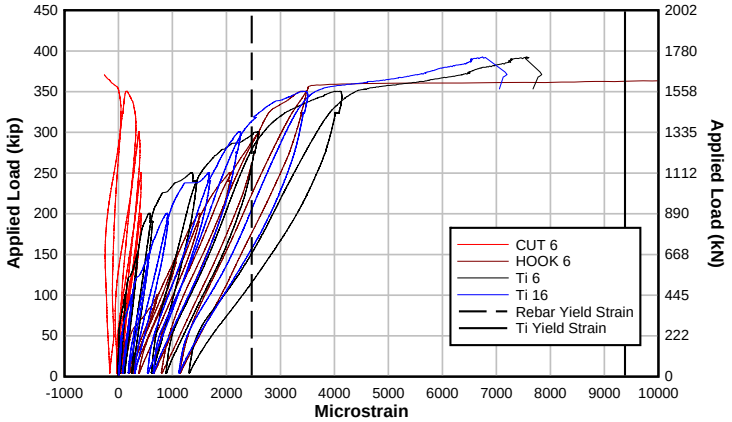

Figure B.23 - T.45.Ld3(10).Ti Section 6 strain

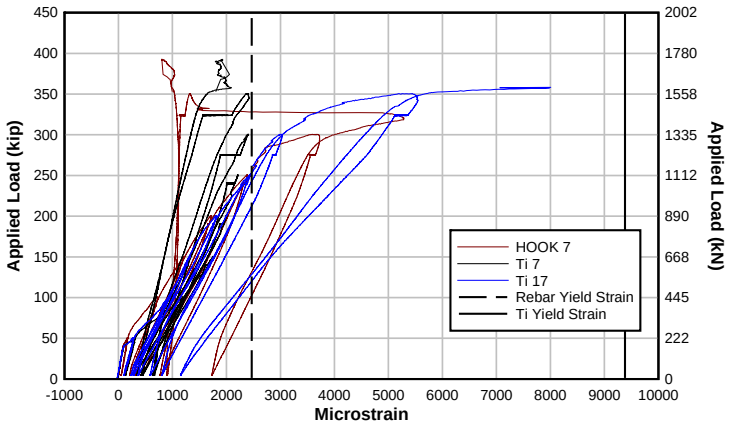

Figure B.24 - T.45.Ld3(10).Ti Section 7 strain

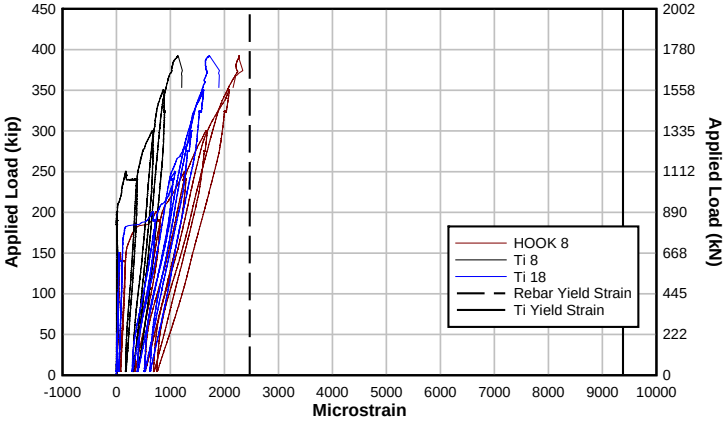

Figure B.25 - T.45.Ld3(10).Ti Section 8 strain

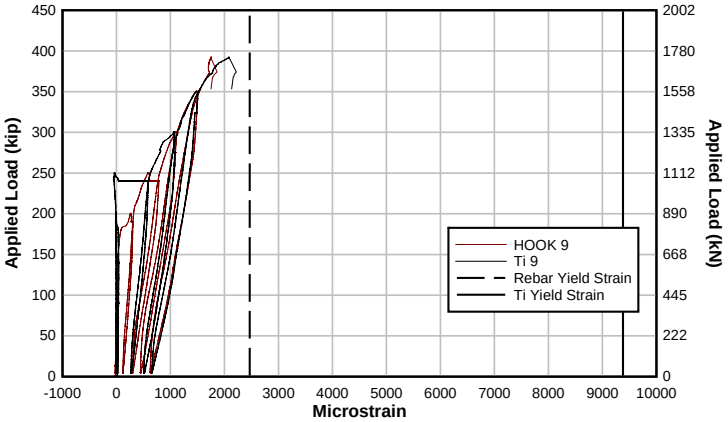

Figure B.26 - T.45.Ld3(10).Ti Section 9 strain

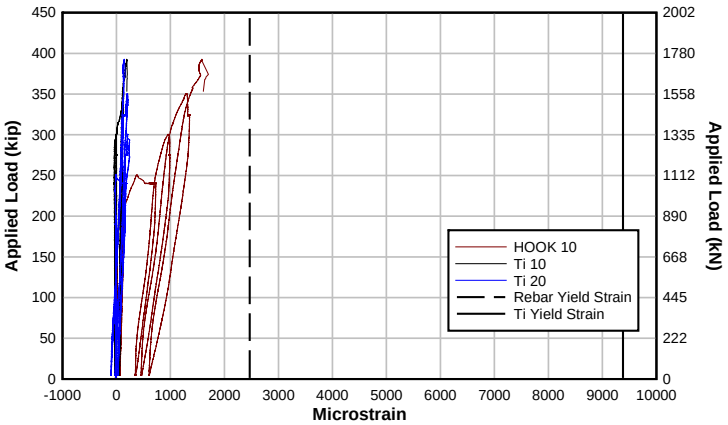

Figure B.27 - T.45.Ld3(10).Ti Section 10 strain

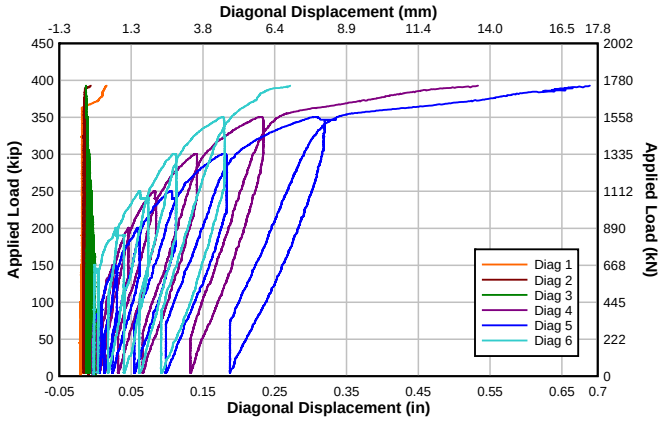

Figure B.28 - T.45.Ld3(10).Ti Diagonal sensor displacement

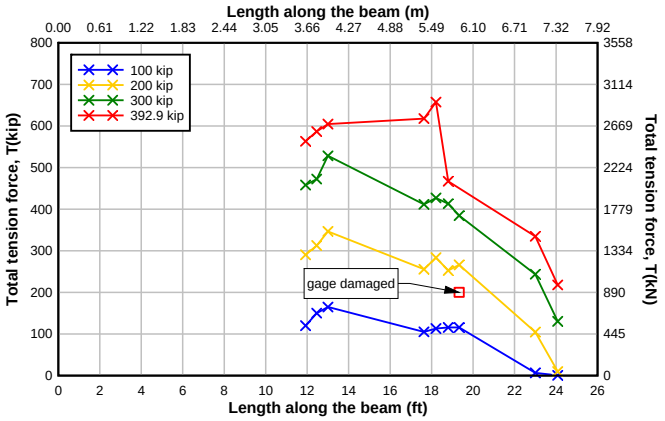

Figure B.29 - T.45.Ld3(10).Ti Flexural tensile force along length at load intervals

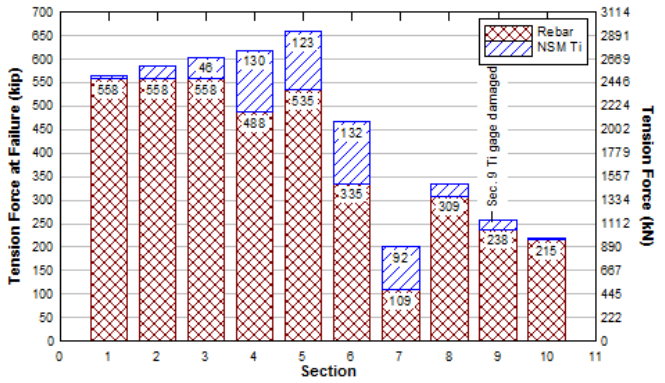

Figure B.30 - T.45.Ld3(10).Ti Steel reinforcing bar vs NSM bar maximum tension force

B.2 T.45.Ld3(6).Ti

Figure B.31 - Specimen T.45.Ld3(6).Ti at failure

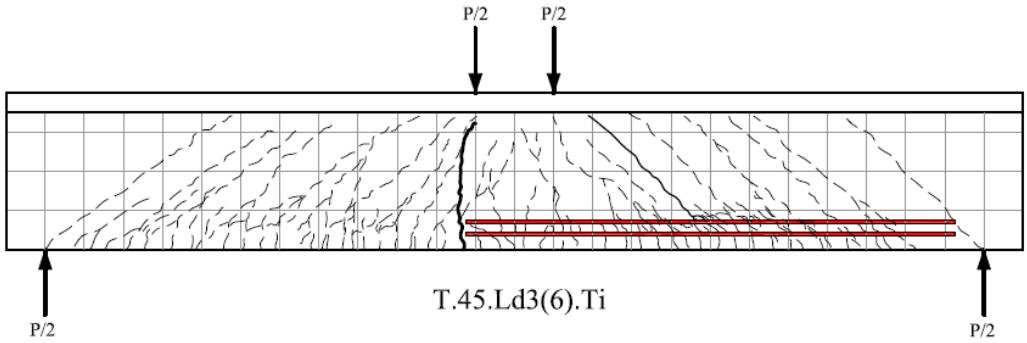

Figure B.32 - Specimen T.45.Ld3(6).Ti crack map

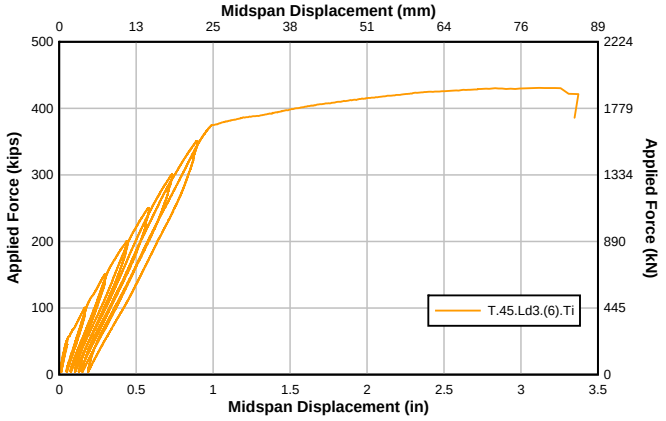

Figure B.33 - Specimen T.45.Ld3(6).Ti Load displacement curve

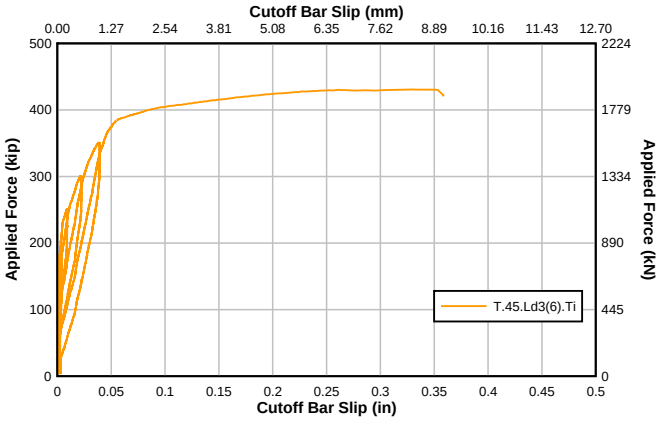

Figure B.34 - T.45.Ld3(6).TI Cutoff bar slip

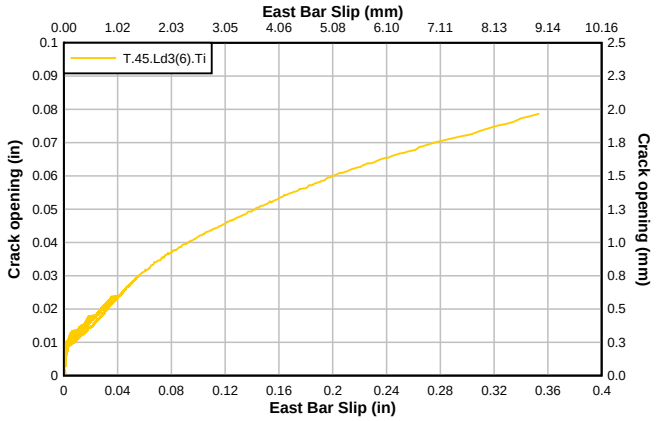

Figure B.35 - T.45.Ld3(6).Ti Crack opening vs cutoff bar slip

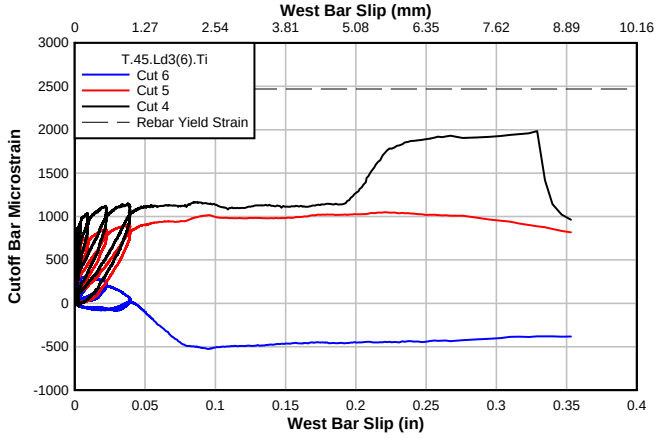

Figure B.36 - T.45.Ld3(6).Ti Slip and cutoff bar strain

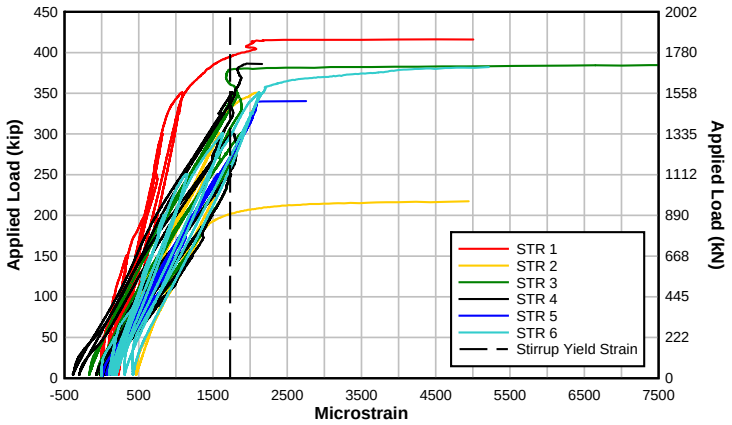

Figure B.37 - T.45.Ld3(6).Ti Strain in stirrups along diagonal crack

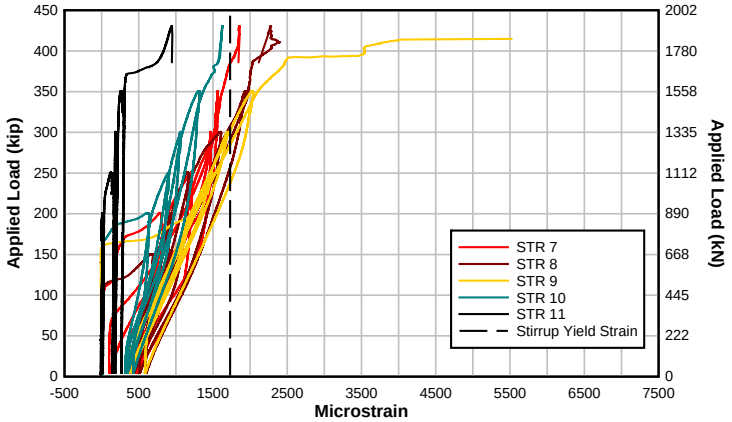

Figure B.38 - T.45.Ld3(6).Ti Strain in stirrups mid height

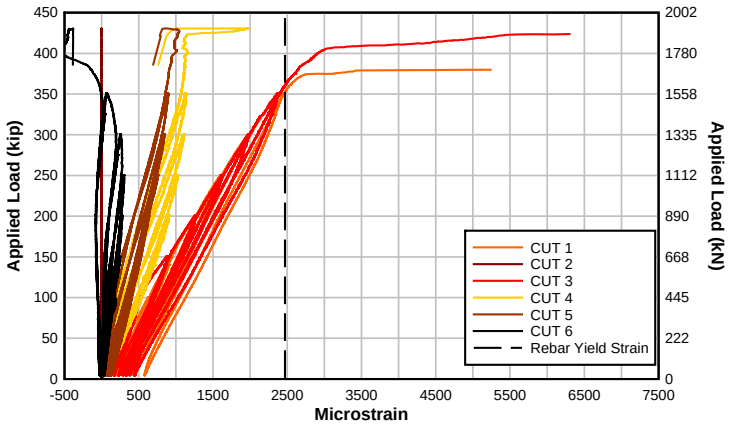

Figure B.39 - T.45.Ld3(6).Ti Strain in cutoff bar

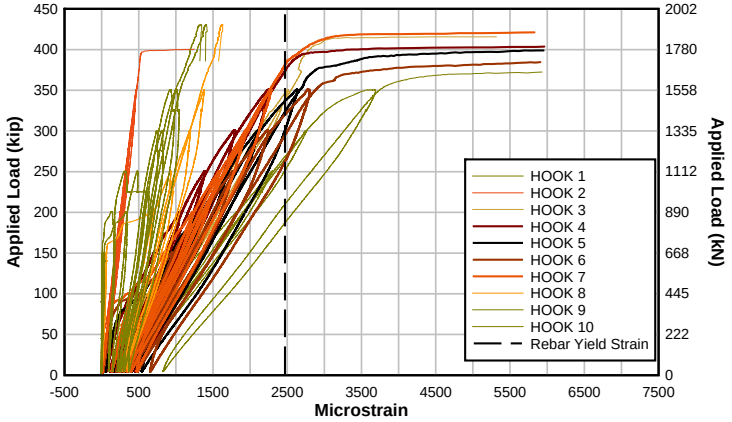

Figure B.40 - T.45.Ld3(6).Ti Strain in hooked bar

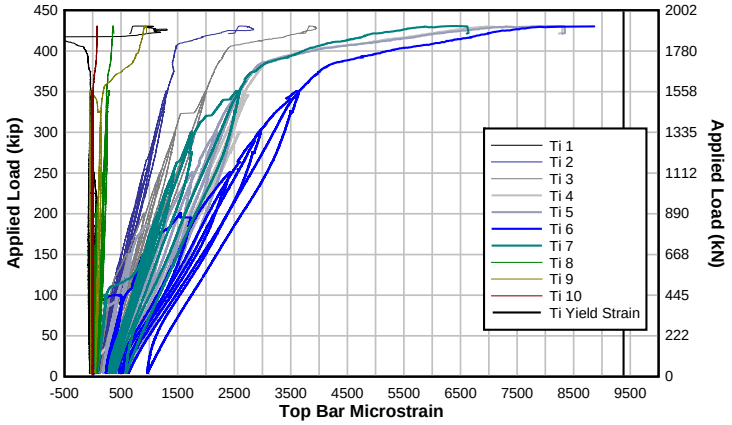

Fig. B.41 - T.45.Ld3(6).Ti Strain in upper titanium bar

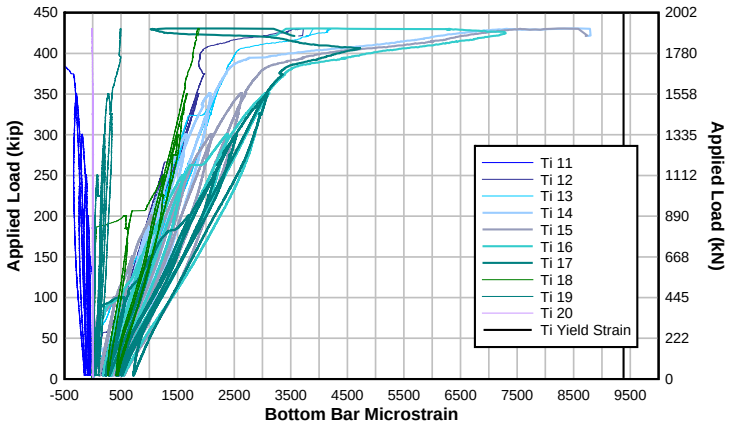

Figure B.42 - T.45.Ld3(6).Ti Strain in lower titanium bar

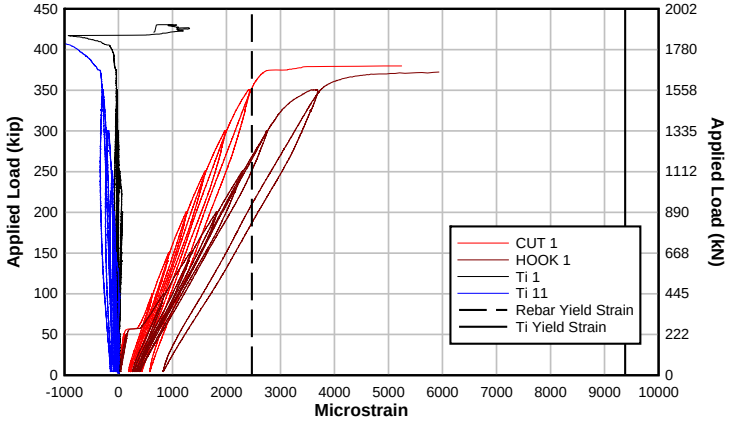

Figure B.43 - T.45.Ld3(6).Ti Section 1 strain

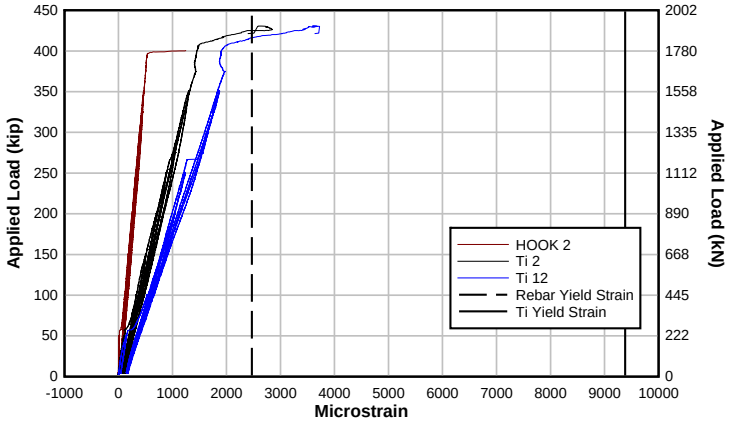

Figure B.44 - T.45.Ld3(6).Ti Section 2 strain

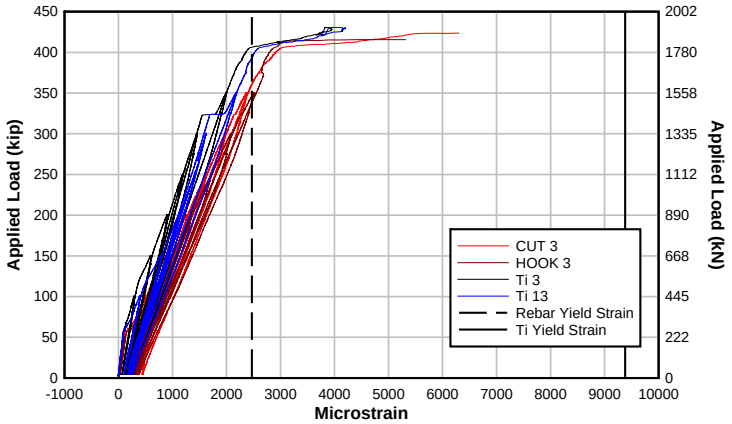

Figure B.45 - T.45.Ld3(6).Ti Section 3 strain

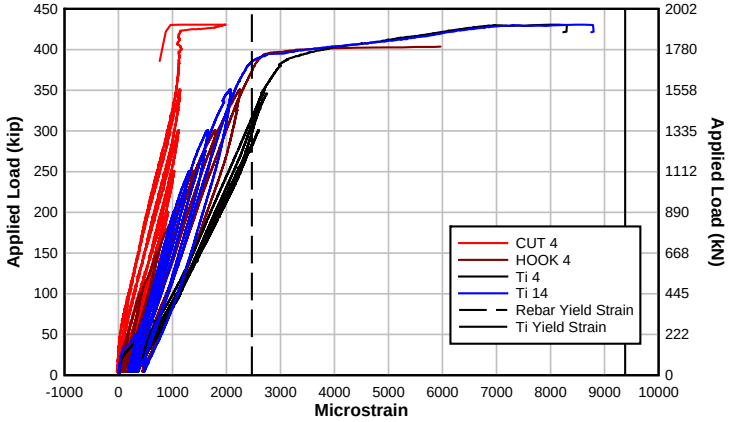

Figure B.46 - T.45.Ld3(6).Ti Section 4 strain

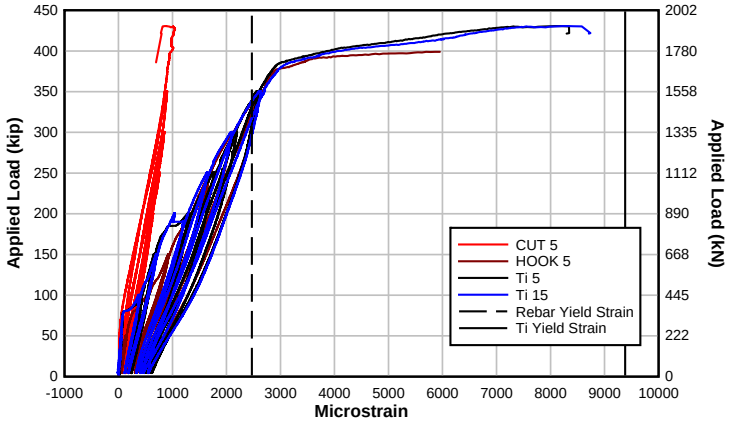

Figure B.47 - T.45.Ld3(6).Ti Section 5 strain

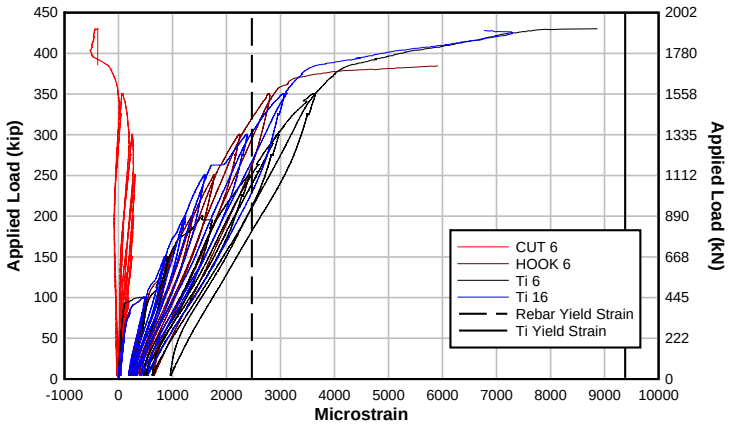

Figure B.48 - T.45.Ld3(6).Ti Section 6 strain

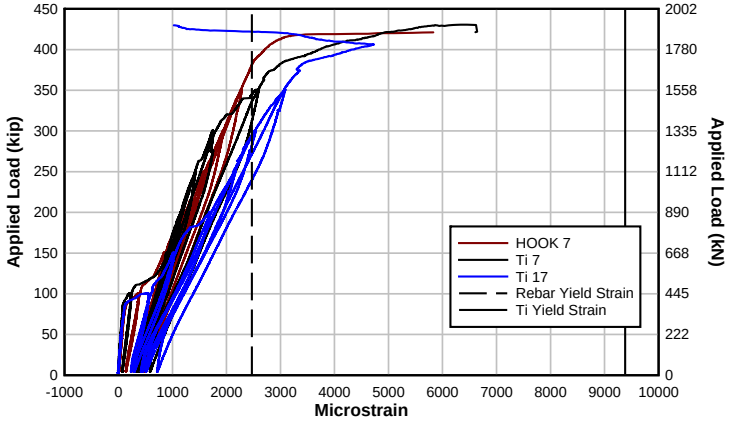

Figure B.49 - T.45.Ld3(6).Ti Section 7 strain

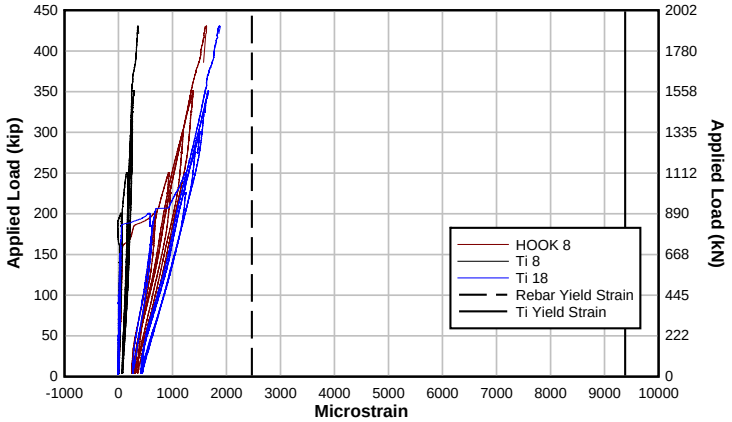

Figure B.50 - T.45.Ld3(6).Ti Section 8 strain

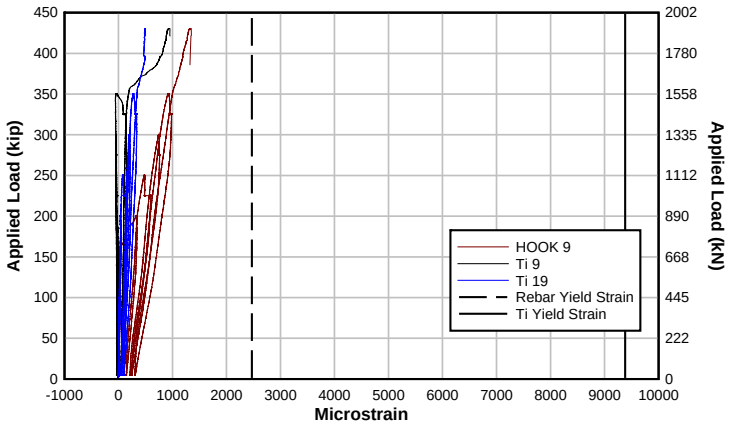

Figure B.51 - T.45.Ld3(6).Ti Section 9 strain

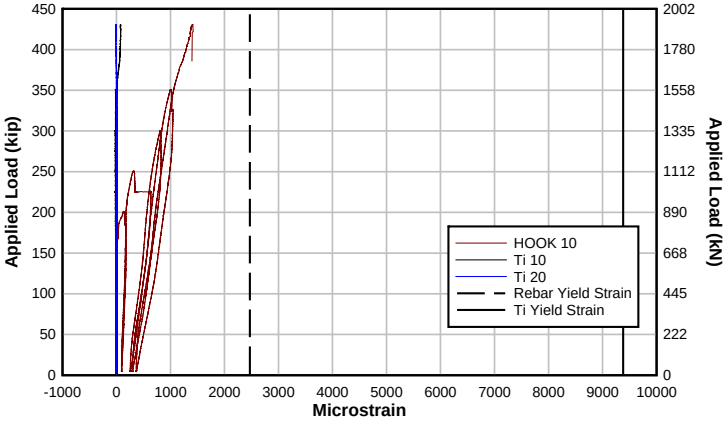

Figure B.52 - T.45.Ld3(6).Ti Section 10 strain

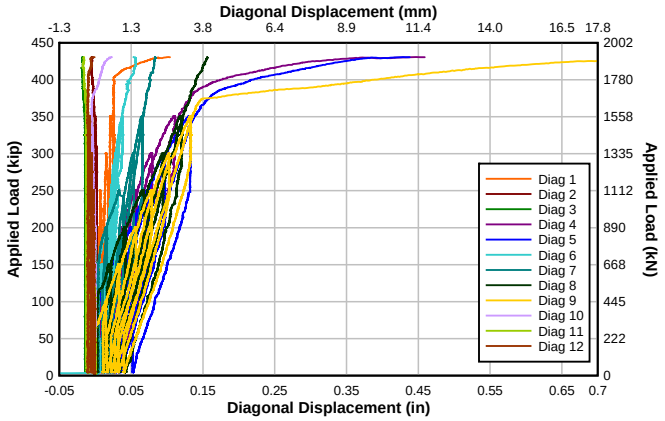

Figure B.53 - T.45.Ld3(6).Ti Diagonal sensor displacement

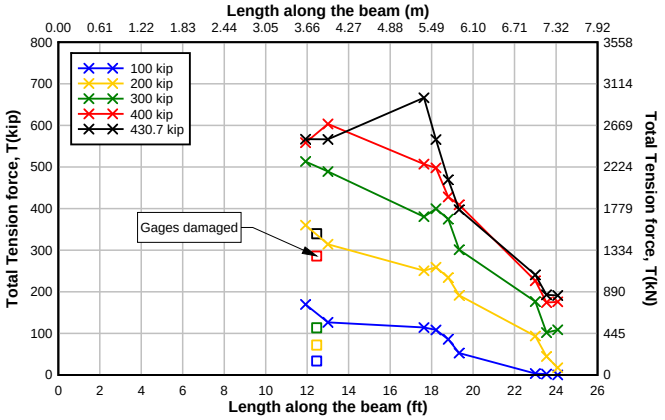

Figure B.54 - T.45.Ld3(6).Ti Flexural tension force along the length at load intervals

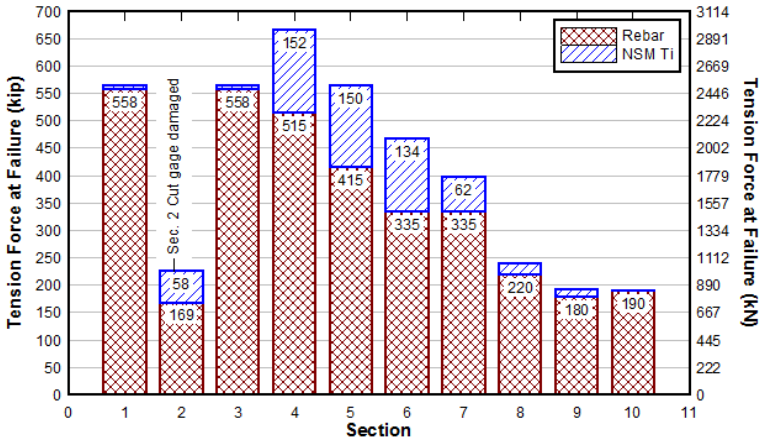

Figure B.55 - T.45.Ld3(6).Ti Steel reinforcing bar vs NSM bar maximum tension force

B.3 T.45.Ld3(6).SS

Figure B.56 - Specimen T.45.Ld3(6).SS

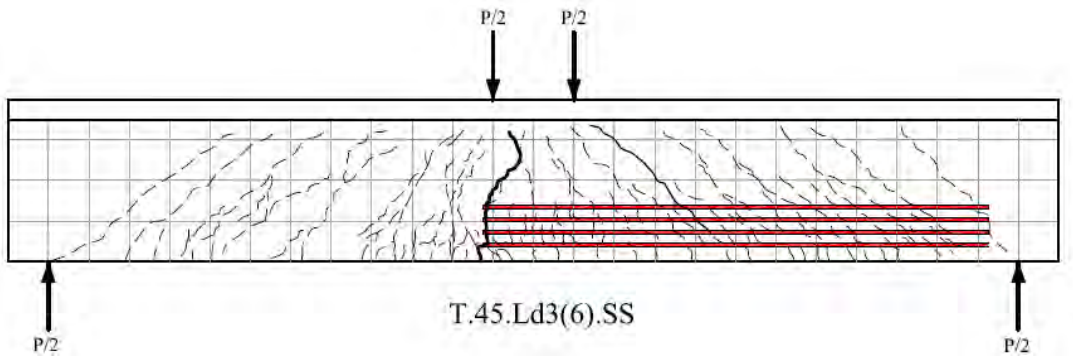

Figure B.57 - Specimen T.45.Ld3(6).SS crack map

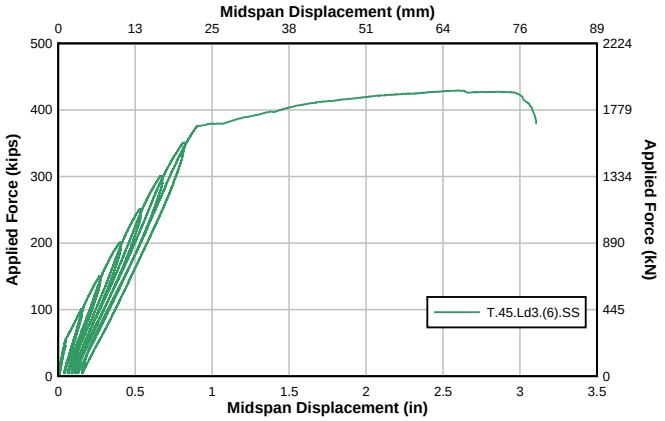

Figure B.58 - Specimen T.45.Ld3(6).SS Load displacement curve

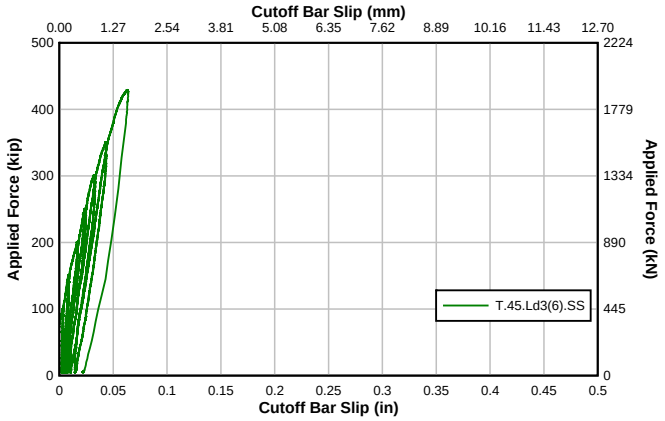

Figure B.59 - T.45.Ld3(6).SS Cutoff bar slip

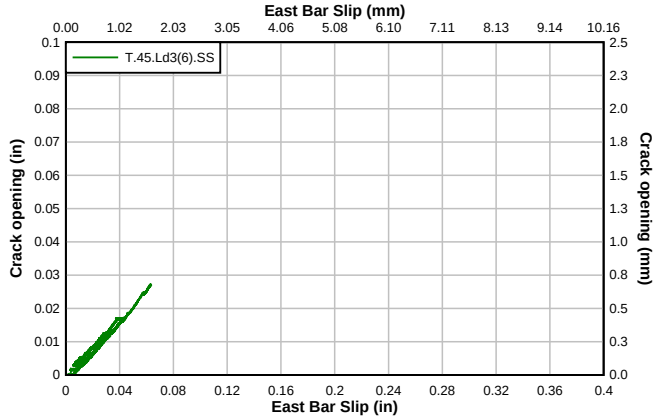

Figure B.60 - T.45.Ld3(6).SS Crack opening and cutoff bar slip

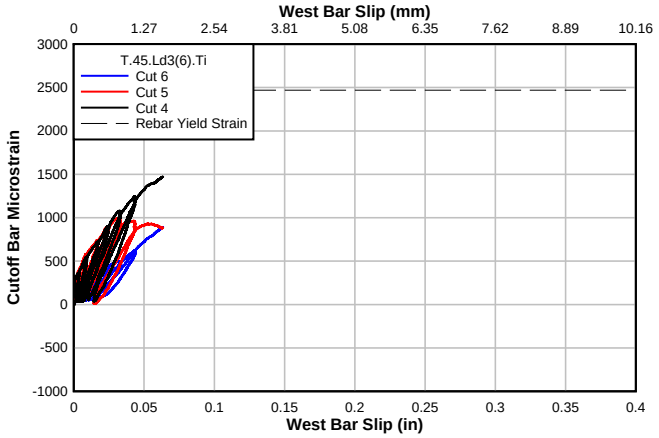

Figure B.61 - T.45.Ld3(6).SS Slip and cutoff bar strain

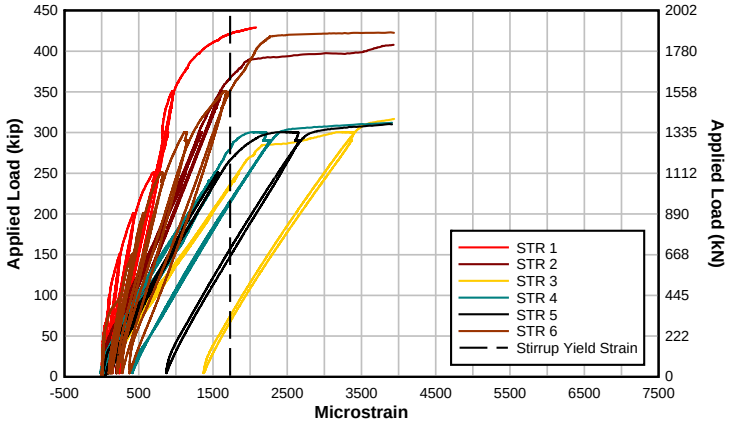

Figure B.62 - T.45.Ld3(6).SS Strain in diagonal stirrups

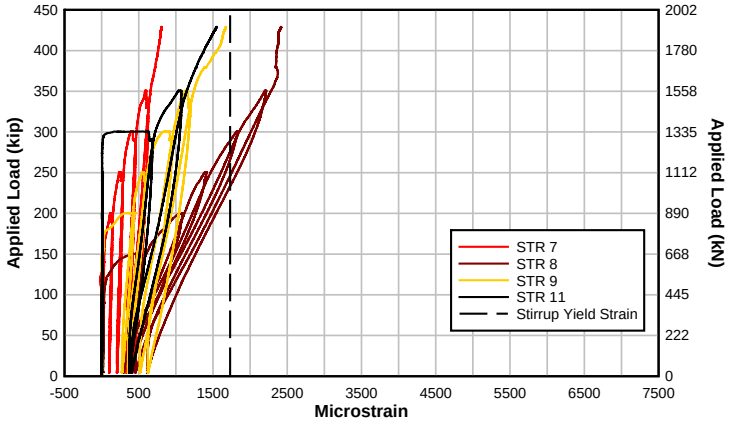

Figure B.63 - T.45.Ld3(6).SS Strain in mid-height stirrups

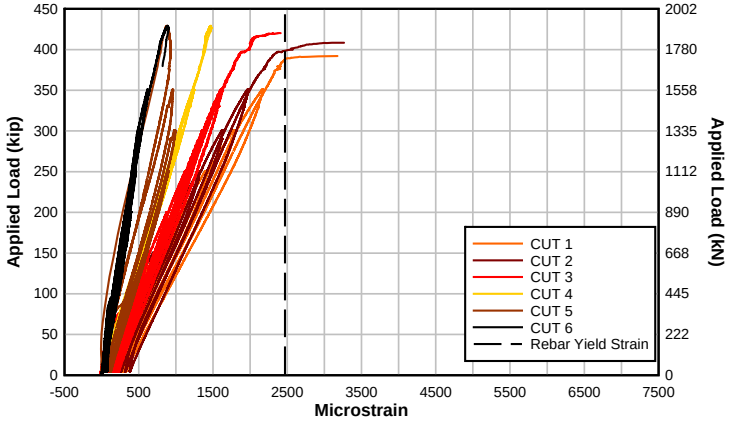

Figure B.64 - T.45.Ld3(6).SS Strain in cutoff bar

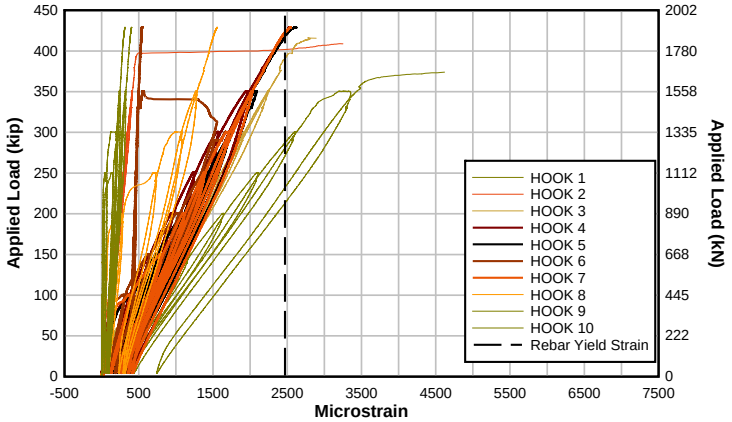

Figure B.65 - T.45.Ld3(6).SS Strain in hooked bar

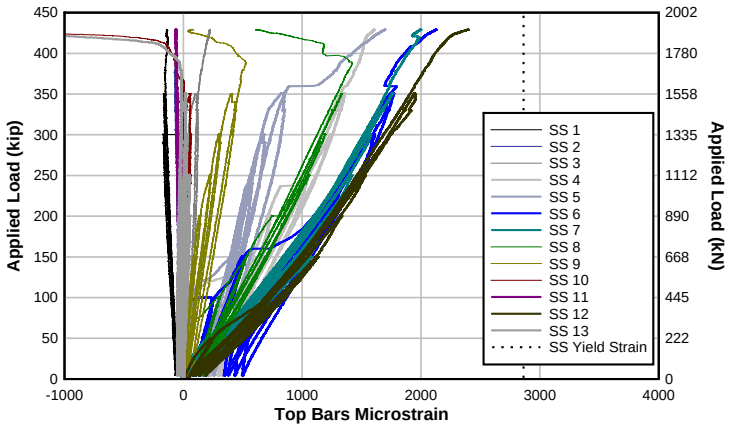

Figure B.66 - T.45.Ld3(6).SS Strain in stainless steel bar 1 & 2

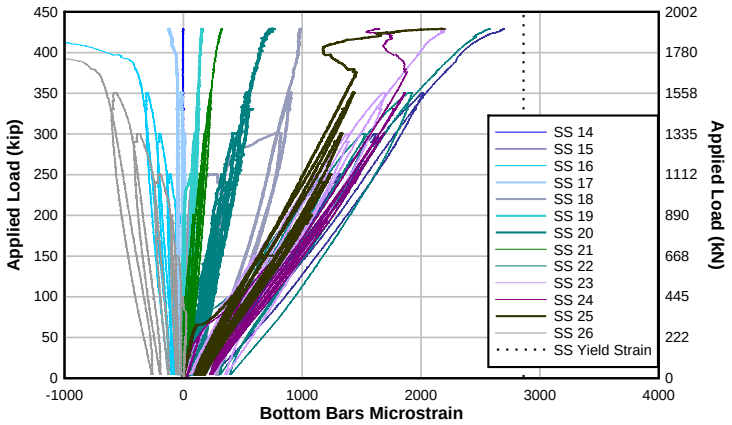

Figure B.67 - T.45.Ld3(6).SS Strain in stainless steel bar 3 & 4

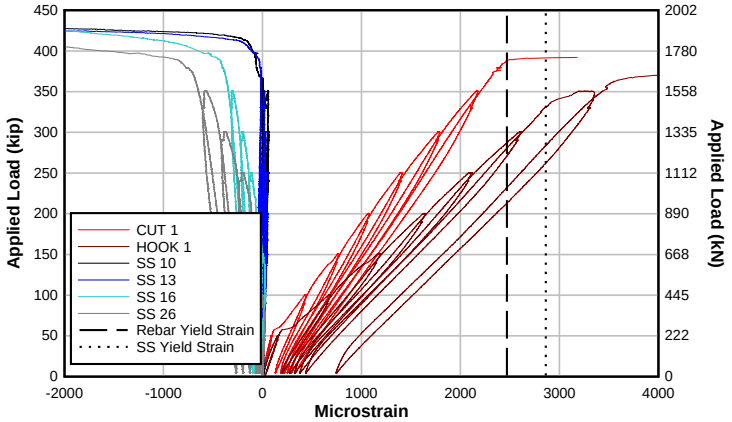

Figure B.68 - T.45.Ld3(6).SS Section 1 strain

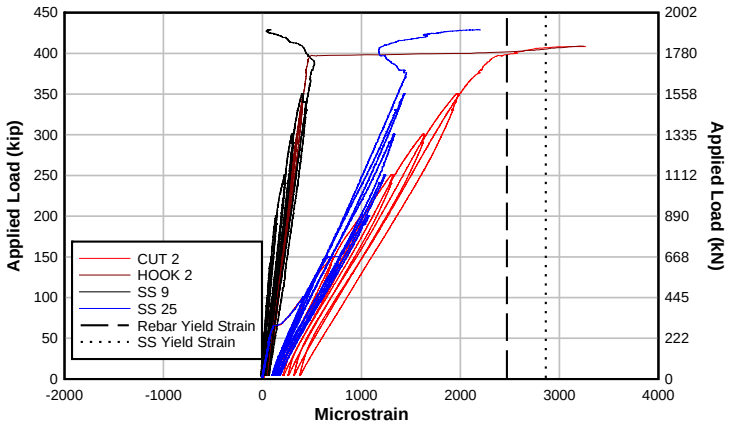

Figure B.69 - T.45.Ld3(6).SS Section 2 strain

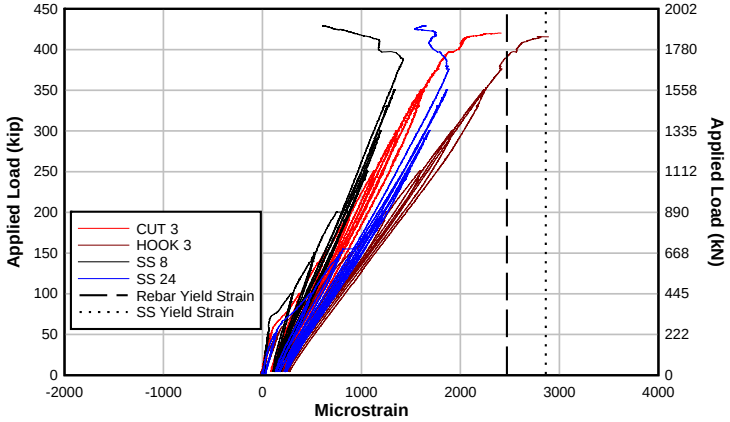

Figure B.70 - T.45.Ld3(6).SS Section 3 strain

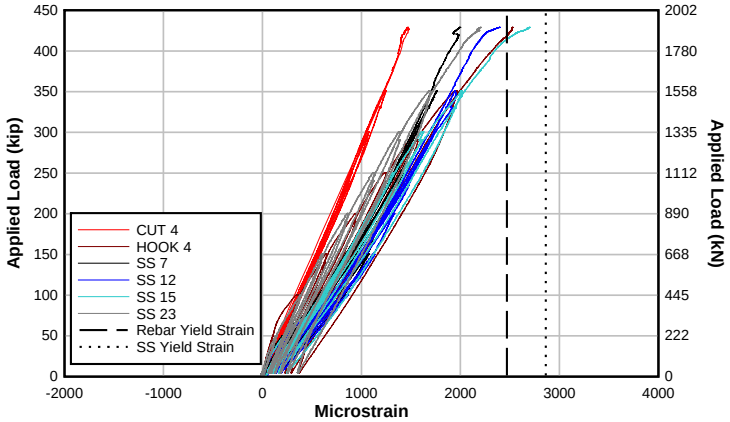

Figure B.71 - T.45.Ld3(6).SS Section 4 strain

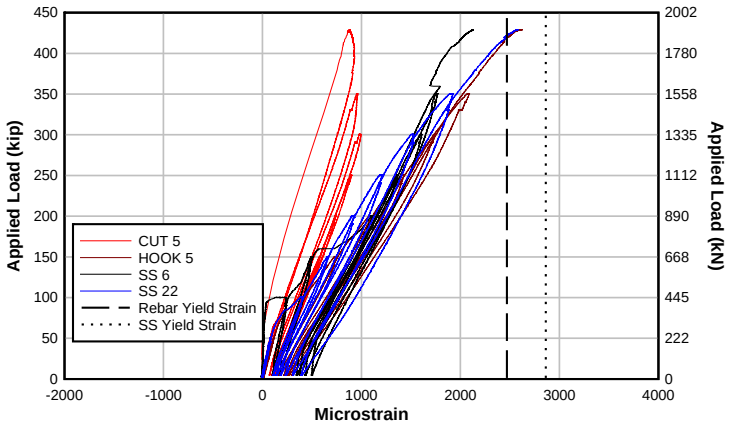

Figure B.72 - T.45.Ld3(6).SS Section 5 strain

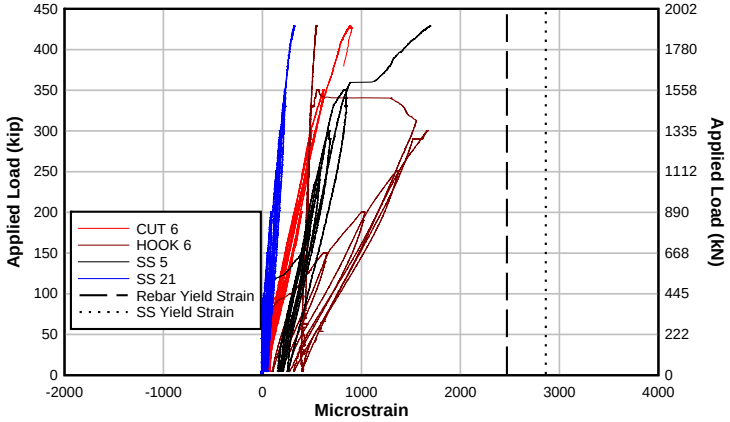

Figure B.73 - T.45.Ld3(6).SS Section 6 strain

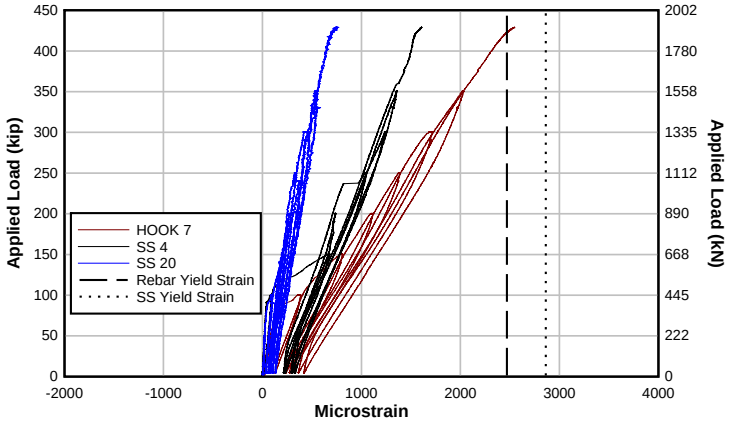

Figure B.74 - T.45.Ld3(6).SS Section 7 strain

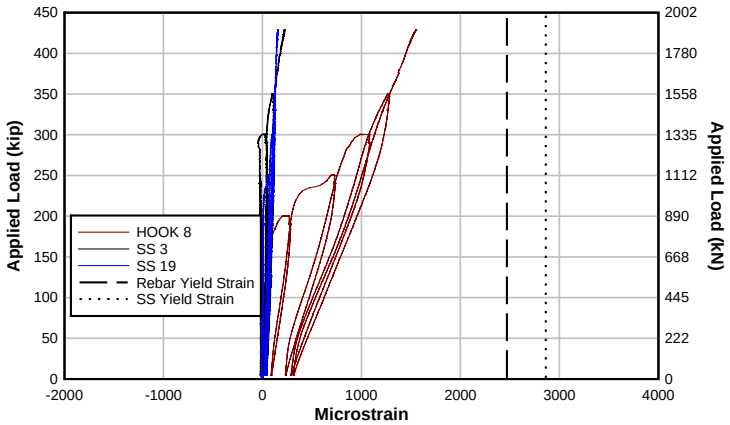

Figure B.75 - T.45.Ld3(6).SS Section 8 strain

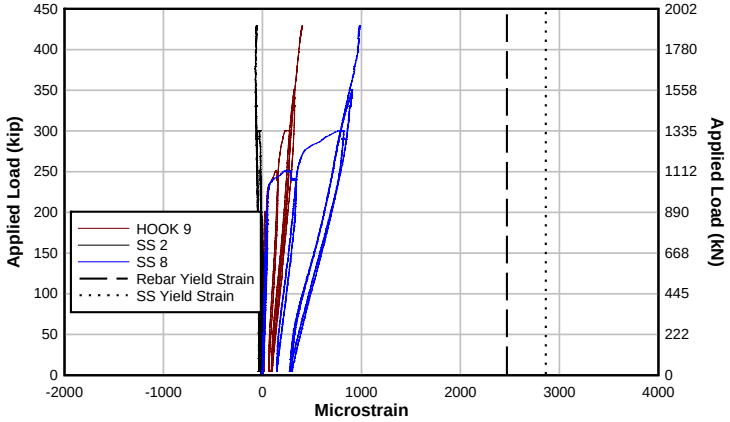

Figure B.76 - T.45.Ld3(6).SS Section 9 strain

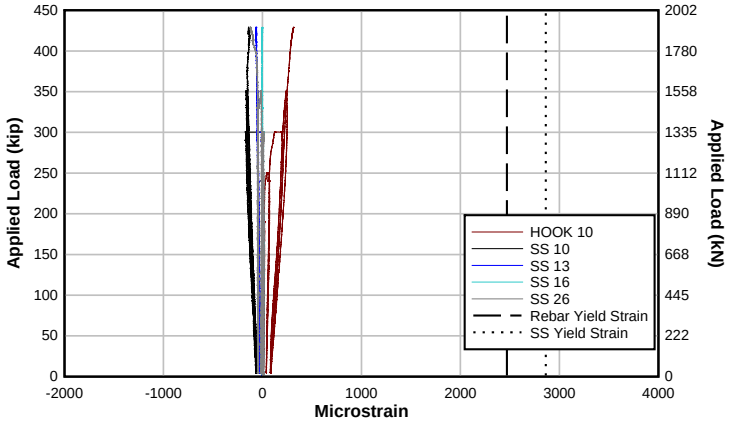

Figure B.77 - T.45.Ld3(6).SS Section 10 strain

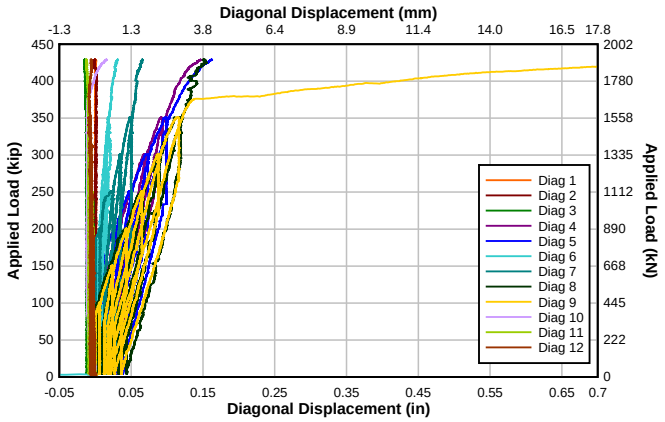

Figure B.78 - T.45.Ld3(6).SS Diagonal sensor displacement

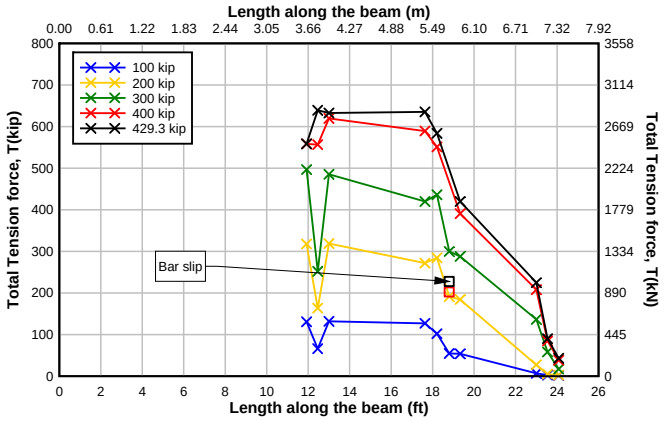

Figure B.79 - T.45.Ld3(6).SS Flexural tensile force along length at load intervals

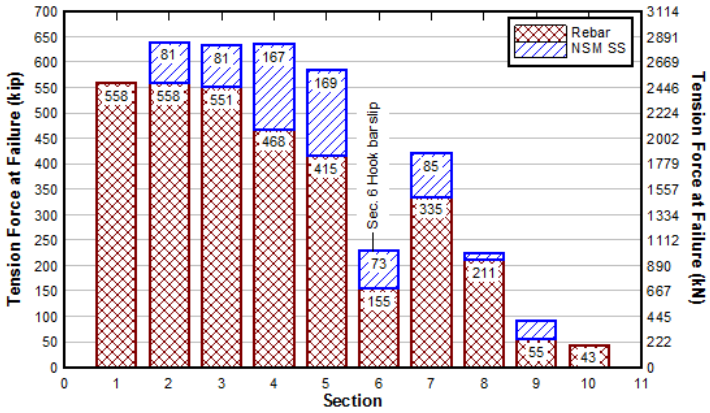

Figure B.80 - T.45.Ld3(6).SS Steel reinforcing bar vs NSM bar maximum tension force

APPENDIX C

MATERIAL PROPERTIES

APPENDIX C – MATERIAL PROPERTIES

C.1 Concrete Mixture Design

Concrete was supplied by a local ready-mix supplier. The mixture design had a 28-day target compressive strength of 3000 psi (21 MPa) which was based on the AASHO "Class A" mixture used for vintage concrete bridges. The concrete used rounded river rock and had a water to cement ratio of 0.55 to imitate concrete mixtures typically used during the 1950's. Water reducing and air entraining admixtures were added for workability. Grace Daravair 1000 was the air entraining admixture and was dosed at a rate of 1.4 oz/yd^3 (54.5 mL/m^3). Grace WRDA-64 was used to reduce the water and was dosed at a rate of 18.8 oz/yd^3 (727.3 mL/m^3). The mixture had a target slump of 5 in. (127 mm). Table C.1 describes the concrete mixture design used for the specimens.

Table C.1 – Typical Concrete Mixture Design

Material	Specific Gravity	Weight lb [kg]	Volume ft^3 [m^3]
Cement	3.15	470 [279]	2.39 [0.089]
Water (Total)	1.00	259 [154]	4.15 [0.154]
3/4 - #4 Round PCC	2.60	1741 [1032]	10.73 [0.397]
Manufactured Sand	2.56	209 [124]	1.31 [0.048]
PCC Sand	2.58	1183 [702]	7.35 [0.272]
Air (4%)		0	1.08 [0.04]
Admixtures	1.00	1 [0.78]	0.02 [0.001]
Total		3863 [2291]	27.00 [1.000]

C.2 Tensile Coupon Results

A 110 kip (489 kN) universal testing machine (UTM) was used for the steel and NSM materials tensile testing. Testing was performed under displacement control and the coupons were loaded at a rate of 0.001 in/sec (0.254 mm/sec) until past visible yield. After yielding, the loading rate was increased to 0.003 in/sec (0.0762 mm/sec). An extensometer measured the strains over the 2 in. (50.8 mm) gage length. To prevent damage, the extensometer was removed before rupture of the bars.

Three coupons each of steel, titanium, and stainless steel were pulled until rupture to measure the yield and ultimate strength of each material. The actual values of yield and ultimate were determined from averaging each set of three tests. The longitudinal steel was Grade 60 (Grade 420), the transverse steel was Grade 40 (Grade 280) and the stainless steel was Grade 75 (Grade 520). The titanium did not have a specified grade. The coupon stress was determined by dividing the applied load by the bar area. The stress-strain diagrams for each the steel reinforcing and NSM materials are shown in below in Figures C.1 and C.2, respectively. Because stainless steel and titanium do not have well-defined yield plateaus, the yield stresses were identified using the 0.2% offset method. Table C.2 shows a summary of the coupon data including yield stress, ultimate strength, and ultimate elongation.

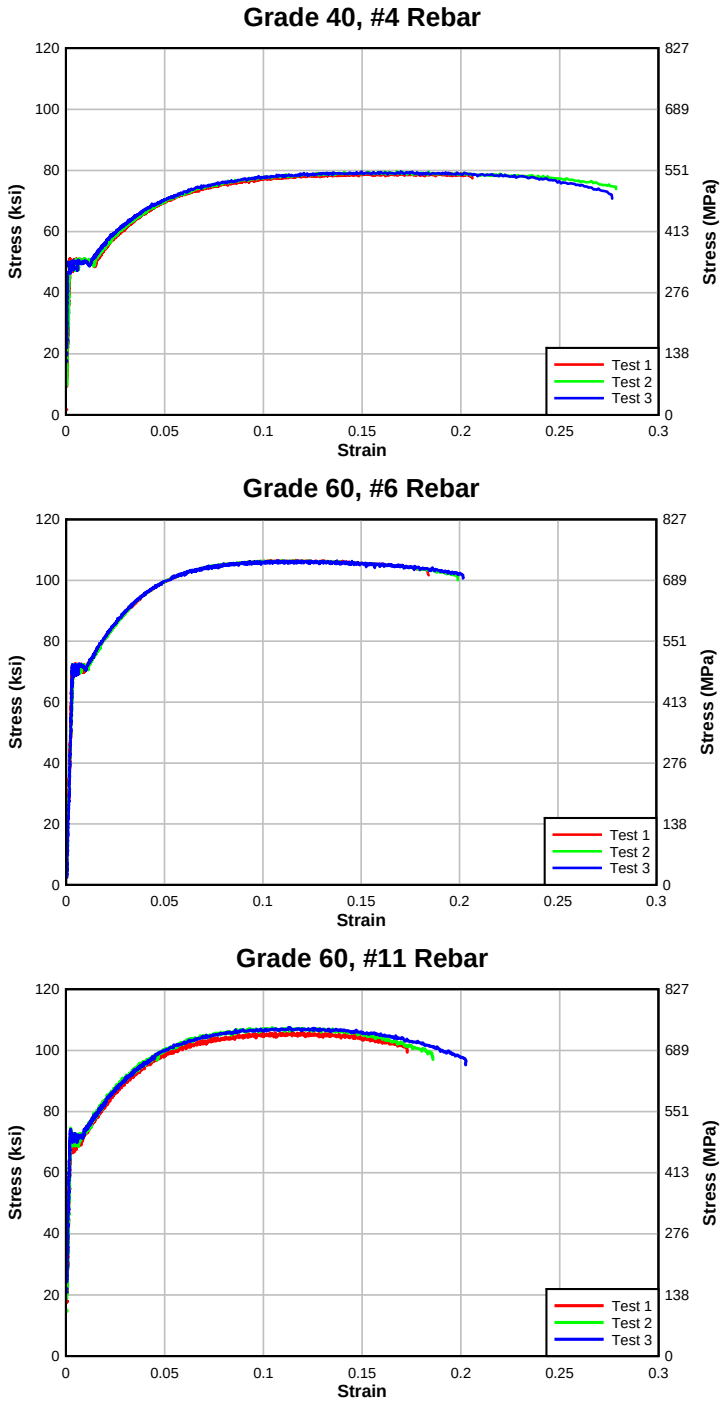

Figure C.1 – Stress-strain curves for steel reinforcement.

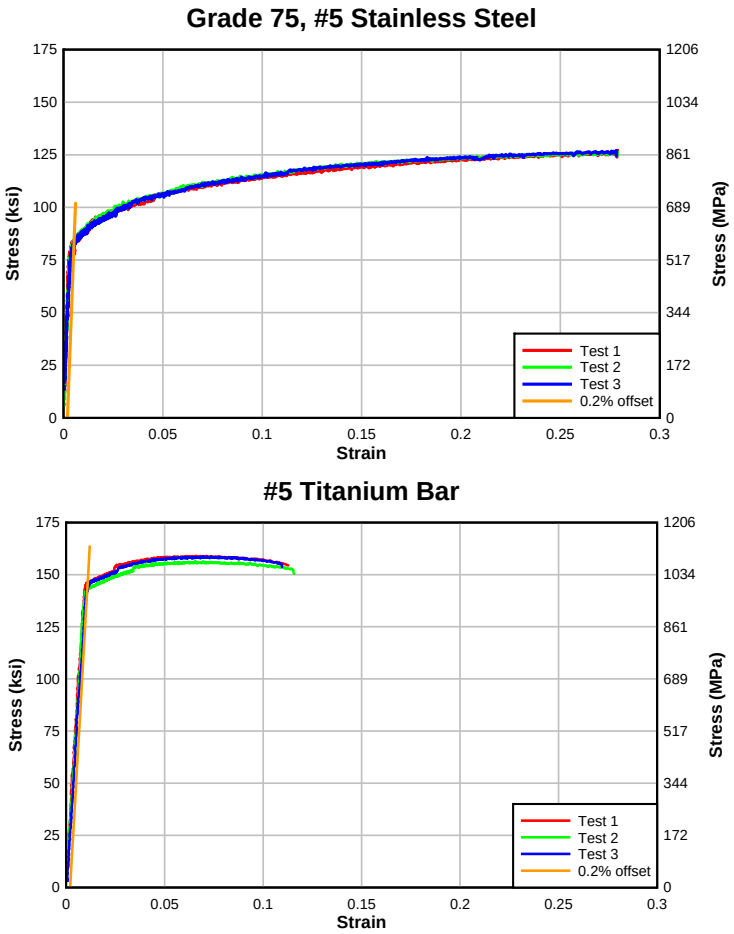

Figure C.2 – Stress-strain curves for NSM reinforcement.

Table C.2 – Summary of coupon data.

Coupon		Yield Stress, f_y ksi [MPa]	Ultimate Strength, f_u ksi [MPa]	Ultimate Elongation, ε_u
Grade 40 #4 Rebar	1	50.3 [347]	79.4 [547]	0.327
	2	50.3 [347]	79.7 [549]	0.282
	3	50.1 [345]	79.7 [549]	0.313
	Average	**50.2 [346]**	**79.6 [549]**	**0.307**
Grade 60 #6 Rebar	1	72.3 [498]	106.7 [736]	0.250
	2	72.1 [497]	106.6 [735]	0.244
	3	72.1 [497]	106.6 [735]	0.296
	Average	**72.2 [498]**	**106.6 [735]**	**0.263**
Grade 60 #11 Rebar	1	70.1 [483]	105.9 [730]	0.229
	2	72.3 [498]	107.5 [741]	0.233
	3	72.4 [499]	107.5 [741]	0.231
	Average	**71.6 [494]**	**107.0 [738]**	**0.231**
Grade 75 #5 Stainless Steel	1	82.5 [569]	127.7 [880]	0.513
	2	83.8 [578]	127.0 [876]	0.442
	3	82.8 [571]	127.3 [878]	0.525
	Average	**83.0 [572]**	**127.3 [878]**	**0.494**
#5 Titanium	1	146.2 [1008]	159.0 [1096]	0.106
	2	143.6 [990]	156.5 [1079]	0.130
	3	146.4 [1009]	158.8 [1095]	0.098
	Average	**145.4 [1002]**	**158.1 [1090]**	**0.111**

APPENDIX D

MOSIER BRIDGE STRENGTHENING

APPENDIX D: MOSIER BRIDGE STRENGTHENING

D.1 Introduction

The Mosier bridge case study was performed at the request of the Oregon Department of Transportation (ODOT). The bridge is an overcrossing of the Columbia River highway (I-84) in the state of Oregon. The Mosier connection serves a nearby quarry and was built in 1953. Typical of practices in the 1950s, the bridge was tapered and haunched to a smaller section at midspan than at the supports. During a routine biennial bridge inspection in 2013, large vertical cracks were observed around known cutoff locations of longitudinal reinforcing steel in an interior girder. The cracks observed had a unique vertical offset and confirmed the need for further investigation. Figure D.1 illustrates the location of the Mosier Bridge over the Columbia River Highway and Figure D.2 shows an elevation view of the bridge and span under question.

Figure D.1- Areal view of Mosier Bridge (Google Maps, 2014)

Figure D.2 - Mosier bridge with highlighted span 1 (Google Maps, 2014)

The Mosier Bridge is a four span reinforced concrete deck girder (RCDG) bridge. The original three spans were built in 1953 and the bridge was lengthened in 1959 (ODOT, 2013). After the bridge inspection identified a 0.03 in. (0.762 mm) wide crack in the North span interior girder, the bridge was shored. Figure D.3a illustrates the observed cracks with vertical offset and Figure D.3b shows the reinforcing steel details superimposed over the image of the crack beam span.

Figure D.3a – View of haunch transition on interior girder of span 1 (right) and crack with vertical offset on interior girder of span 1(left) (ODOT 2013)

Figure D.3b – Overlay of reinforcing steel details on image of cracked girder.

Analysis of the Mosier Bridge was conducted using a line analysis of the continuous span bridge and sweeping the ODOT prescribed rating truck models over the span. The moment distribution factor was 0.872 and the impact factor was 1.2. The maximum factored moment was computed as 284.9 kip-ft (386.3 kN-m) and was produced by the Continuous Trip Permit 3 (CTP3) truck having a live load factor of 1.3. The live load places the deck into compression over the critical section. The service-level dead load moment (using a load factor of 1.0) at the section was computed as -68.9 kip-ft (93.4 kN-m) which puts the deck into tension. These essential features were accommodated into the experimental design as described subsequently. Combining the factored live load moment and service-level dead load moment, the demand at the critical section was 219 kip-ft (297 kN-m). The calculated moment demand is 46 kip-ft (63 kN-m) above the AASHTO design moment capacity. The corresponding shear resulting from factored live load and service-level dead load was 60.5 kips (269 kN), which results in a M/V ratio of 3.6 ft (1.1 m).

The very low bridge rating and visual distress observed by inspections required immediate shoring to maintain traffic and then strengthening. Near-surface mounted (NSM) titanium, stainless steel, and CFRP were considered for the strengthening of the Mosier Bridge. However,

due to geometric constraints, the titanium alloy bars were determined as the most cost effective retrofitting material.

D.2 Experimental Program

An experimental program was developed to strengthen anchorage deficiencies and flexural strength in a full-scale positive moment T-specimen to simulate a strengthening procedure on the Mosier Bridge. The specimens were constructed, strengthened, and tested to failure to evaluate the effectiveness of the NSM titanium strengthening. The experimental program details the specimen design, details, material properties, instrumentation, and test protocol of the Mosier specimens.

D.2.1 Specimen Design

Mosier specimen design was based on the as-built details from the Mosier bridge drawings. The girder evaluated and strengthened in this program was the interior girder of span 1 shown in Figure D.2. Similar to the Mosier Bridge girders, the specimens included a slight taper and haunch detail at midspan. Analysis of the span in consideration determined that the dead load produced negative moments, and live load produced positive moments at the haunch location. To simulate this, a unique test protocol was created described in Section *D.2.5 Test Protocols.* The clear span of the Mosier specimens was selected to match similar shear and moment demands at the haunch location in the Mosier Bridge. To further simulate conditions of the existing bridge similar concrete strengths and reinforcing steel strengths were selected. Specimen strengthening methodology was similar to the NSM titanium strengthening techniques described in the body of the report.

Three specimens were constructed in the Mosier Bridge experimental program: Mosier 1, the as-built specimen, Mosier 2, the NSM titanium strengthened specimen after failing reinforcing steel anchorage, and Mosier 3, the NSM titanium strengthened specimen with reinforcing steel anchorage fully intact. Since the reinforcing steel cutoff details are detailed poorly, the designer would assume zero anchorage from the end of the reinforcing bars to the cracks evident in the Mosier Bridge. Mosier 2 would verify the strengthening process with the assumption that the ends of the flexural steel at midspan are not anchored.

D.2.2 Specimen Details

Simulating in-situ conditions required several unique details when constructing and testing the Mosier specimens. All specimens were 18 ft (5.49m) long and had a 6.5 x 36 in. (165 x 914 mm) deck. The stem was 9 x 29.5 in. (229 x 749 mm) in half of the specimen then transitioned to a cross section of 12.63 x 41.25 in (321 x 1048 mm) through horizontal and vertical tapering after midspan. The reinforcing steel selection and configuration was unique to the Mosier bridge and described in detail in Section *D.2.2.1 Reinforcing Steel.* Construction and NSM strengthening methods were similar to those detailed in Chapter 4 of the report.

D.2.2.1 Reinforcing Steel

Reinforcing steel configurations were determined from the design drawings from 1953. The drawings indicated the reinforcing steel bars were square and also had lower yield strengths than steel commonly used today. Therefore, lower yield, smaller bars were used for construction of the Mosier specimens. Anchorage lengths and dimensions of the flexural steel from design drawings were used to detail the Mosier specimens. Figure D.4 and Figure D.5 display the elevation and cross sections from the 1953 drawings of the girder being considered.

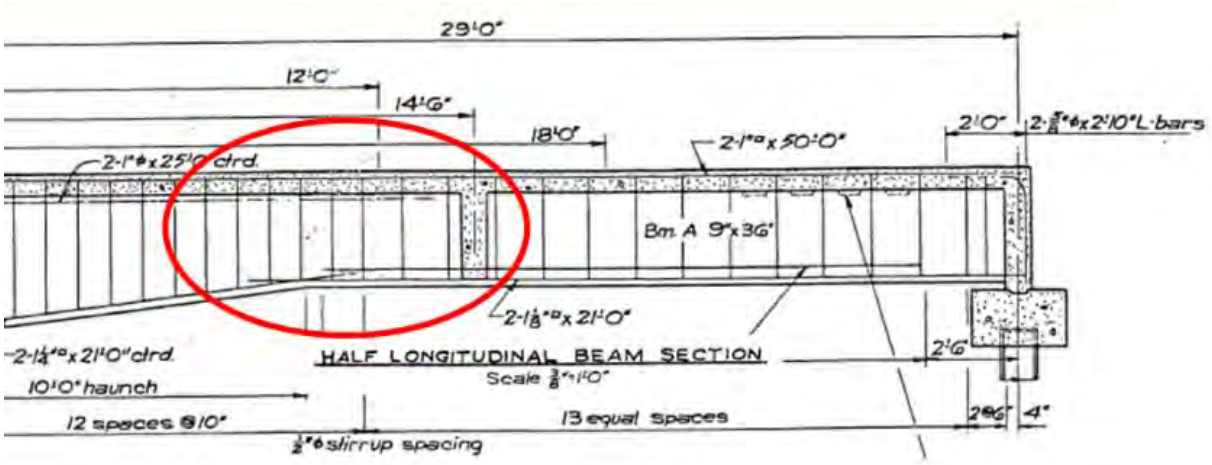

Figure D.4 – As-built elevation drawing of Mosier Bridge with highlighted critical section (ODOT 2013)

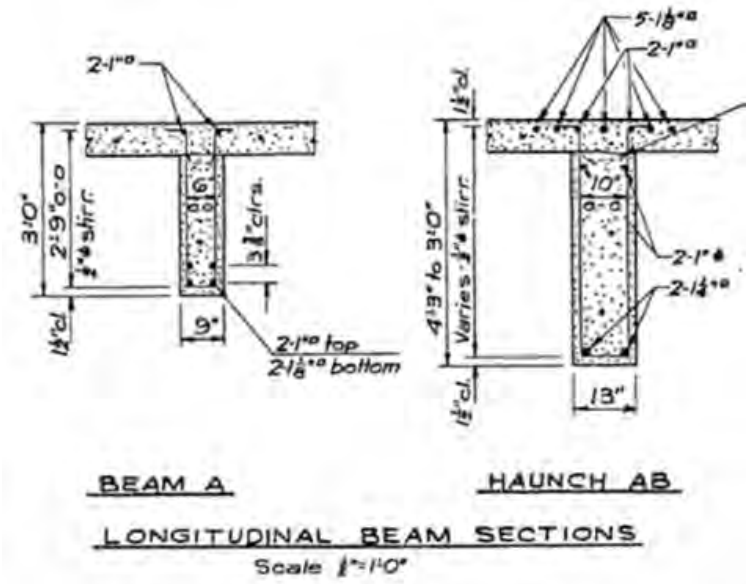

Figure D.5 – As-built cross section of Mosier Bridge span 1 interior girder (ODOT 2013)

The haunch intersection with vertical offset cracks in the Mosier Bridge is highlighted in Figure D.4. Beam A in Figure D.5 is the smaller, constant cross section in Mosier specimens for 9 ft (2.74 m). The Mosier specimen transitions to Haunch AB in the remaining 9 ft (2.74 m).

All specimens had identical longitudinal reinforcing steel. Longitudinal reinforcing steel in the web consisted of two #7 (22M) and two #8 (25M) bars on the South half and two #9 (29M) bars through the North half. Two #6 (19M) steel reinforcing bars were located in the upper stem on the North end. All longitudinal reinforcing steel bars were adequately anchored past the support locations. To resist negative moments, the Mosier specimens had two #7 (22M) and five #8 (25M) steel reinforcing bars in the flange terminating at various lengths. Double-legged, open #4 (13M) stirrups were spaced 12 in. (305 mm) on center throughout midspan in Mosier 1 and Mosier 2. Mosier 3 decreased the stirrup spacing before the NSM titanium strengthening initiated. Figure D.6 through Figure D.12 display the cross section, elevation, and plan drawings for the Mosier specimens built in this experimental program.

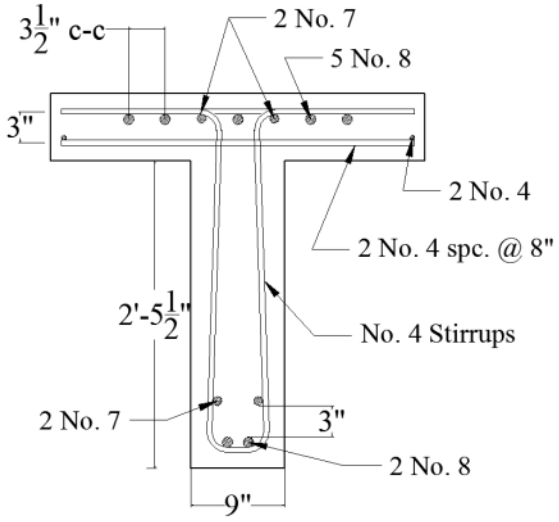

Figure D.6 – Cross section at South end of Mosier specimen.

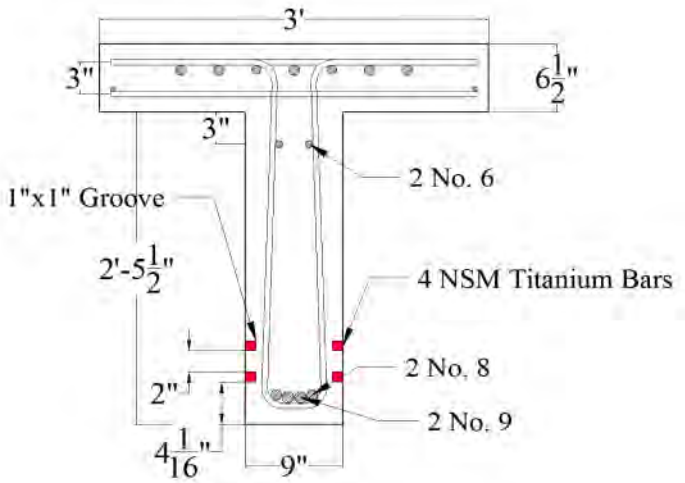

Figure D.7 - Cross section at midspan of Mosier specimen with NSM Titanium.

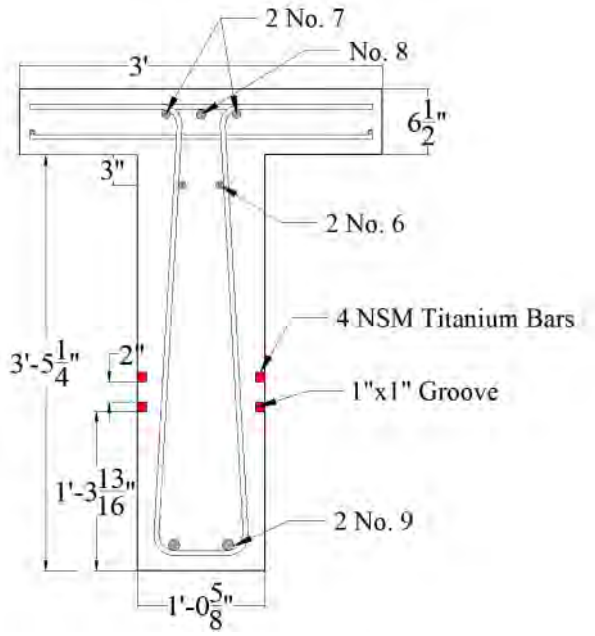

Figure D.8 - Cross section at North end of Mosier specimen with NSM Titanium.

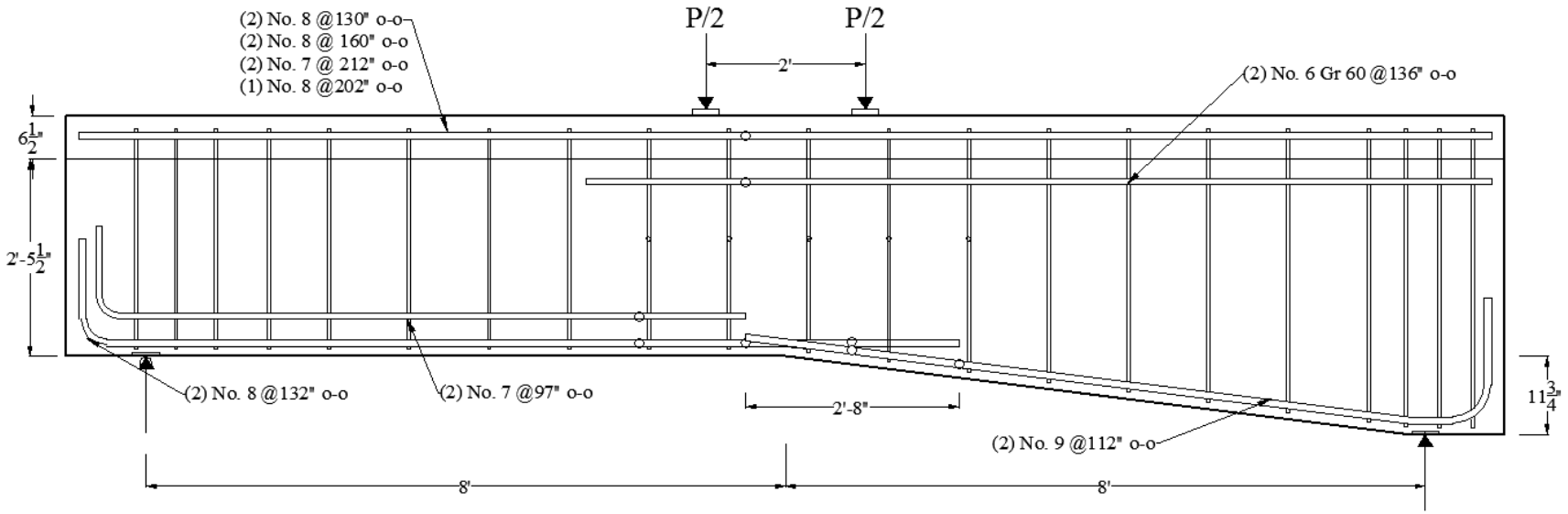

Figure D.9 - Elevation of Mosier 1

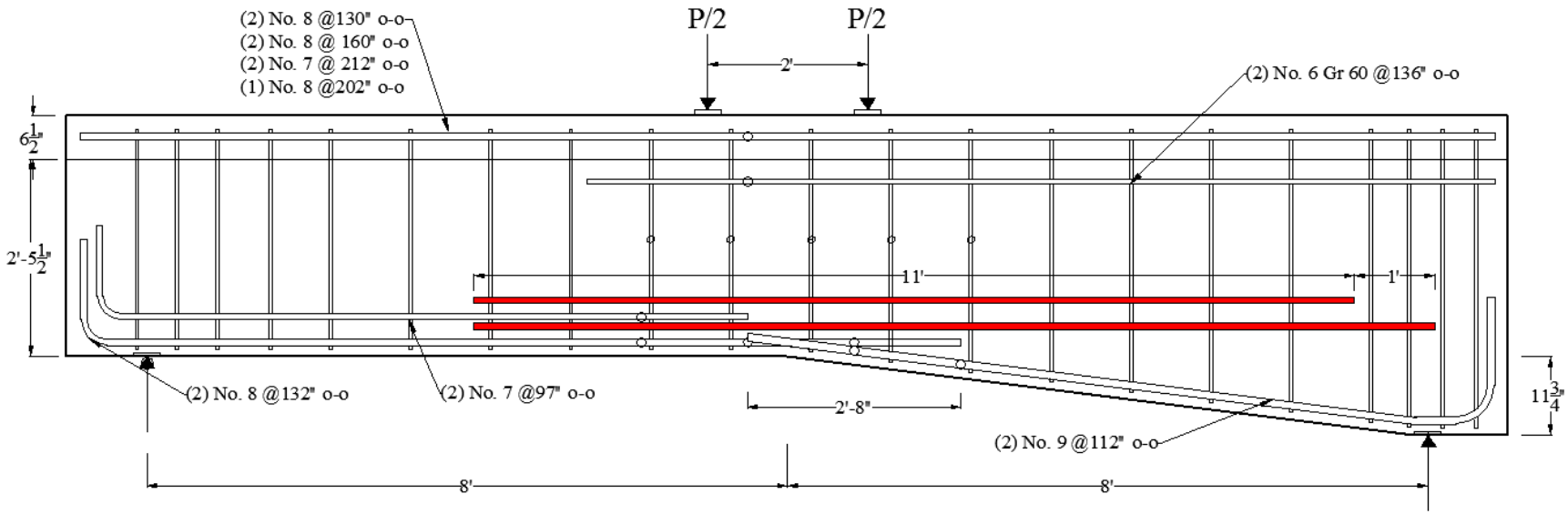

Figure D.10 - Elevation of Mosier 2 with NSM titanium

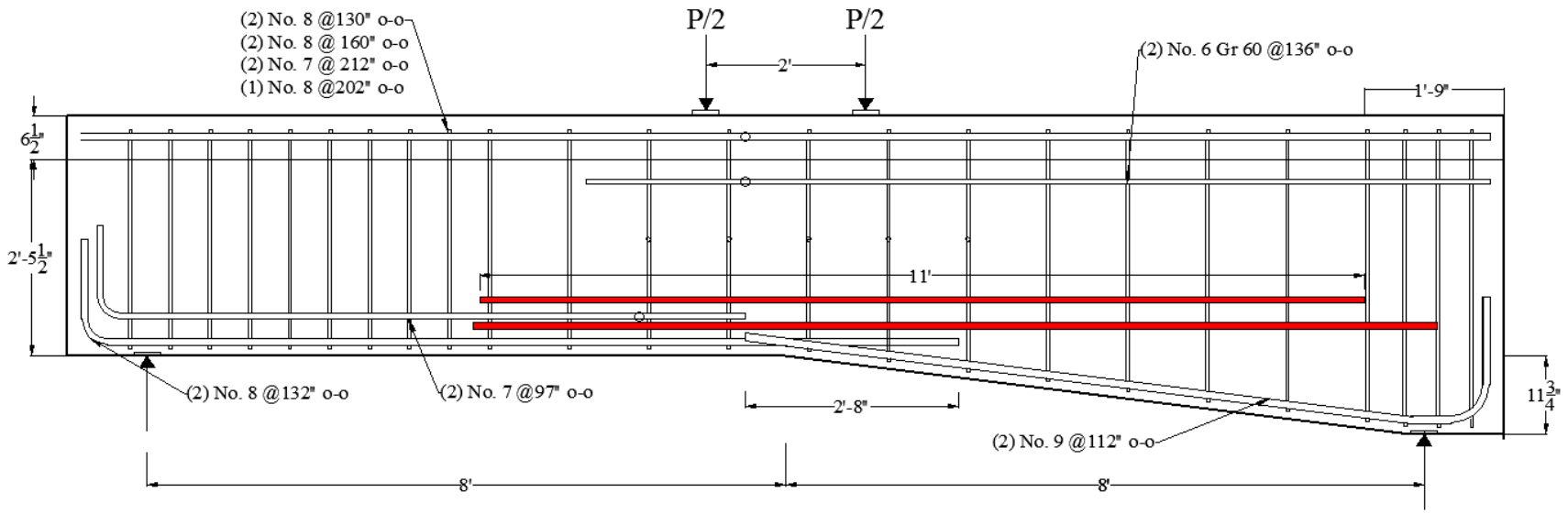

Figure D.11 - Elevation of Mosier 3 with NSM titanium

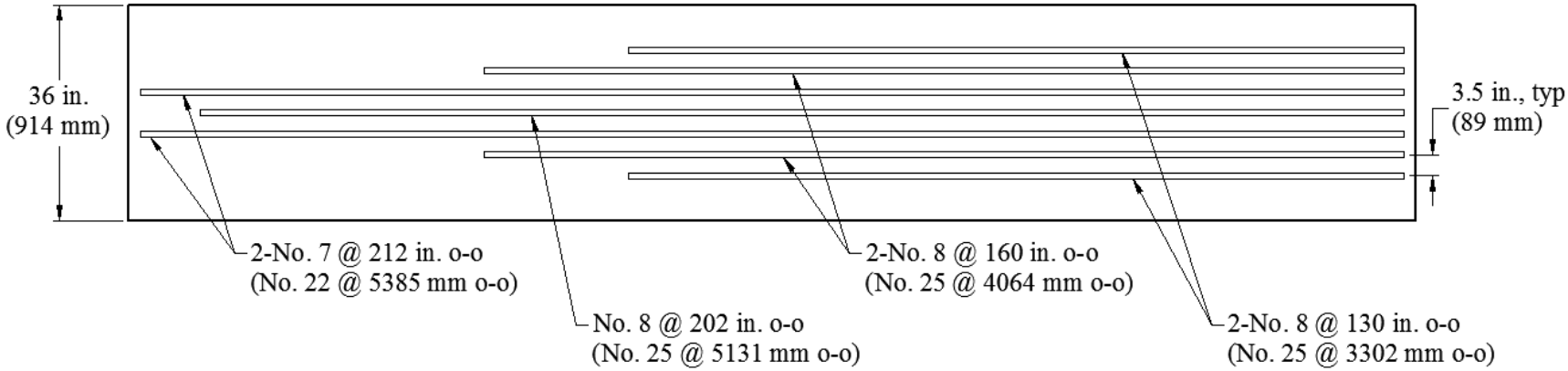

Figure D.12 Plan view of steel in deck of all Mosier specimens.

The cross section drawings show the longitudinal reinforcing steel and NSM titanium for applicable specimens. The cross section at midspan was congested with four steel reinforcing bars in close proximity. The most deficient detail in the Mosier specimens was the overlapping of the #8 (25M) and #9 (29M) bars at midspan. While the as-built drawing suggested more overlap, in reality the two bars are developing simultaneously at the point of maximum moment. Mosier 3 decreased stirrup spacing and terminated the NSM titanium bars at slightly different locations than Mosier 2. The upper and lower NSM titanium bars were shifted 1 in. (25.4 mm) relative to each other.

D.2.2.2 Construction

The construction of the Mosier specimens initiated after strain gage sensors were applied to the internal reinforcing steel as described in Section *D.2.4.2 Internal Sensor Array*. This section describes the cage construction, the preformed crack details, and the concrete casting process.

The longitudinal bars were cut to length and bent on site using a bar bending machine. Stirrups of increasing height were ordered from a local reinforcing bar fabricator. To create the steel reinforcing cage, stirrups spaced 12 in. (305 mm) apart or tighter were hung from the steel reinforcing bars in the deck. Two #8 (25M) steel reinforcing bars were tied to the stirrups for the lower layer of flexural reinforcement on the South half of the Mosier specimens. Similarly, two #9 (29M) steel reinforcing bars were tied to the tapered stirrups as the flexural reinforcement on the North half. At midspan the two #9 (29M) steel reinforcing bars intersected the two #8 (25M) steel reinforcing bars as shown in Figure D.12. The cutoff layer of #7 (22M) steel reinforcing bars were spaced 3 in. (76.2 mm) clear from the top of the #7 (22M) layer. Several 1.5 in. (38 mm) wide spacers were attached to the stirrup legs and longitudinal steel to provide sufficient cover. Figure D.13 pictures the completed reinforcing steel cage for Mosier 1.

Figure D.13 - Midspan reinforcing steel terminations for Mosier specimens

Figure D.14 - Mosier 1 reinforcing steel cage

In Mosier 1, a block-out was placed around the ends of the #7 (22M) steel reinforcing bars to measure the bar end slip. Mosier 2 did not measure the #7 (22M) reinforcing bar end slip because the anchorage was failed prior to testing on purpose to fulfill the design intent. Mosier 3 did not include a block-out around the #7 (22M) reinforcing bar ends.

To achieve the specified dimensions, the Mosier formwork was tapered and haunched using falsework in a larger T-specimen form. Once the specimens were fully instrumented and constructed, the reinforcing cages were placed in the formwork. Concrete was supplied by a local ready-mix provider. Concrete was placed into a bucket then placed into the forms using an overhead crane. Care was taken to avoid the internal instrumentation while the concrete was consolidated with a mechanical vibrator. The specimens were finished and cured for seven days. After initial curing, the specimens were removed from the formwork and placed in a stable configuration for the saw-cutting the grooves for the NSM retrofit.

D.2.2.3 NSM Details and Installation

The design intent of NSM material strengthening procedure is to retrofit anchorage deficiencies and provide additional flexural capacity in the Mosier Bridge. To accomplish this, the reduction in flexural strength where the #8 (25M) and #9 (29M) steel reinforcing bars are developing must be bridged. To increase the Mosier Bridge capacity and maintain posted ratings, the flexural reinforcing must be fully developed at midspan through the addition of the NSM material. NSM strengthening design methodologies detailed in Chapter 3 of the report were utilized in this case study.

The NSM titanium alloy bar selected had a 0.61 in. (15.5 mm) diameter with a nominal yield stress of 145 ksi (1000 MPa). Using nominal tensile properties, the predicted addition to flexural capacity was found. To increase the positive moment ultimate strength, four NSM titanium bars were required. A 6 in. (152.4 mm) hooked development length was assumed for the titanium alloy NSM materials. The extent of the NSM reinforcing was determined by the existing Mosier Bridge elements. A diaphragm was present at the South end of the interior girder, approximately 5 ft (1.5 m) from the South end of the Mosier specimen; therefore, the NSM titanium was terminated at least 2 in. (51 mm) before the diaphragm to allow for drilling clearances. The NSM titanium alloy on the North end of the Mosier 2 and Mosier 3 specimens was terminated after the exiting the flexural tension zone. The upper layer of NSM titanium alloy bars was terminated prior to the lower layer to minimize a stress concentration. In summary, the strengthening required two NSM titanium alloy bars at a length of 11 ft (3.35 m) out-to-out, and two NSM titanium alloy bars at a length of 12 ft (3.65 m) out-to-out.

NSM groove depth and spacing requirements were determined by ACI 440.2R-08. The groove depth and width was 15/16 in. (23.8 mm) using a #5 (16M) NSM bar. The clear distance between grooves was approximately 3 in. (76.2 mm). The elevation of the NSM titanium alloy was determined by the optimizing the effectiveness of the titanium (providing a large lever arm) and being spaced over the #7 (22M) reinforcing steel bar.

After initial curing, the Mosier 2 and Mosier 3 specimens were placed in a stable configuration for saw-cutting the NSM grooves. Three longitudinal passes were made with a concrete saw. A roto-hammer was used to chip the grooves to their intended depth, and then holes for the hook were drilled using a 3/4 in. (19 mm) diameter drill. The corner between the NSM groove and

circular hole was chiseled to allow for the bend radius of the hook. The NSM titanium was anchored using a 2 in. (51 mm) diameter 90° hook. Due to the width of the stem, the 6 in. (152 mm) hook could not be used if the NSM titanium alloy bars terminated at the same location on each side of the stem. Mosier 2 used a smaller length of hook in the thinner South stem and the 6 in. (152 mm) hook length in the North stem. Mosier 3 used 6 in. (152 mm) long hooks on all ends of the NSM titanium. To allow for the increased hook length in Mosier 3, the NSM titanium bars were offset 1 in. (25.4 mm) on each side of the stem so the hooks would not intersect. The NSM titanium hooks were fabricated in a bar bending machine around a 2 in. (51 mm) diameter pin. Prior to bending, the NSM titanium was heated to a maximum of 900 °F (482 ˚C) with an acetylene torch for all Mosier 2 hooks. The NSM titanium hooks of Mosier 3 were heated to at least 1250 °F (677 ˚C)..

Installation of the Mosier specimens NSM titanium was unique. The dead load of the Mosier Bridge produced negative moments in the section, therefore, the Mosier specimens must experience negative moments prior to and during the NSM titanium installation. A description of this unique loading scheme is described in Section *D.2.5 Test Protocols.* After the specimen was at the specified load to produce negative moments, the load was held. Grooves were cleaned and the epoxy was extruded into the groove before the bar was installed. The bars were held flush within the groove at the haunch transition by a clamp at midspan. The groove was filled with epoxy and finished. Epoxy was cured for a minimum of seven days before unloading the dead load and applying the actuator load.

To fulfill the design intent of the Mosier 2 specimen, the anchorage of the reinforcing steel at midspan was failed prior to installing the NSM titanium. A dynamic actuator load of over 40 kips was applied the Mosier 2 specimen through four point loading. The applied load brought the Mosier 2 specimen near to a flexural failure. The cracking around the anchorage was similar to the cracks seen in the Mosier Bridge. Cracked, unbonded concrete was removed from the anchorage region of the intersecting reinforcing steel bars at midspan. To ensure a monolithic response of the strengthened specimen, the cracks from pre-failing the anchorage were epoxy injected. Once the epoxy injection material was cured the Mosier 2 specimen followed the testing protocols of Mosier 1 and Mosier 3.

The design intent of the Mosier 3 specimen was to test the NSM titanium strengthened specimen with all reinforcing bars fully embedded in the concrete. Additionally, the NSM titanium was confined at the haunch transition at midspan with two steel plates. A confinement plate would resist the outward force induced on the NSM titanium bars from the haunch transition geometry. The outward force on the NSM titanium could be approximately 1 kip (4.89 kN). The dimensions of the steel confining plates were 1/2 x 3 x 15 in. (13 x 76 x 381 mm). The plate was attached with two 1/2 in. (13 mm) diameter steel bolts. A hole was drilled through the stem above the NSM titanium groove at midspan for the steel bolt.

D.2.3 Material Properties

The concrete mix design described in Chapter 4 of the report was used in the Mosier specimens. The concrete mixture design had a specified 28-day compressive strength of 3000 psi (20.68 MPa) and was designed to simulate vintage mixture proportions and materials. Test day concrete strengths from three replicate 6x12 in. (152x305 mm) cylinders for each of the Mosier specimens are listed in Table D.1 below.

Table D.1 - Concrete properties for Mosier specimens

Specimen	f'_c (psi) [MPa]	Standard Deviation (psi) [MPa]	f_{ct} (psi) [MPa]	Standard Deviation (psi) [MPa]	Concrete Age (days)
Mosier 1	3038 [21.0]	76.9 [0.53]	348 [2.40]	25.2 [0.17]	33
Mosier 2	3629 [25.0]	244 [1.68]	275 [1.90]	216 [1.49]	63
Mosier 3	3344 [23.1]	426 [2.94]	353 [2.43]	16.1 [0.11]	58

Test day compressive strengths were determined using the standard test method ASTM C39-12a. Cylinders for split tensile strengths were also crushed on the test date according to ASTM C496-11.

Lower grade, larger diameter steel was typically used in mid-century bridge construction. For the Mosier specimens, smaller Gr. 60 (Gr.420) reinforcing steel was used to follow development length of the intermediate grade steel used in the Mosier Bridge. To best match the actual strength curves of the Mosier bridge, the longitudinal steel was selected based on mill certifications from the reinforcing steel supplier. The longitudinal reinforcement consisted of Gr. 60 (Gr. 420) steel reinforcing bars that conformed to ASTM A706-09. The transverse reinforcement consisted of Gr. 40 (Gr. 280) stirrups and conformed to ASTM A615-09. Table D.2 lists the reinforcing steel material properties for the Mosier specimens.

Table D.2 - Reinforcing steel bar properties for Mosier specimens

Material	Bar Diameter (in.) [mm]	Bar Area ($in.^2$) [mm^2]	Grade (ksi) [MPa]	Actual f_y (ksi) [MPa]	Actual f_u (ksi) [MPa]
Transverse #4 [13M]	0.500	0.20	40	50.2	79.6
	[12.7]	[12.7]	[280]	[346]	[549]
Longitudinal #6 [19M]	0.750	0.44	60	63.0	106.3
	[19.1]	[248]	[420]	[434]	[733]
Longitudinal #7 [22M]	0.875	0.60	60	65.3	104.6
	[22.2]	[387]	[420]	[450]	[721]
Longitudinal #8 [25M]	1.000	0.79	60	63.6	112.1
	[25.4]	[509]	[420]	[438]	[773]
Longitudinal #9 [29M]	1.128	1.00	60	62.6	102.0
	[28.7]	[645]	[420]	[432]	[703]

Procedures from ASTM E8-13a were used to establish yield, ultimate, and elongation values for all samples. To measure strain in the coupon, an extensometer with a 2 in. (50.8 mm) gage length was used. The universal testing machine held an initial loading rate of 0.001 in/sec (0.025 mm/sec) until yield, and then increased subsequently afterward.

The titanium NSM reinforcing material has several unique properties and was chosen because of its high strength, ductility, environmental durability and ability to bend around a tight radius. The titanium alloy has 6% aluminum and 4% vanadium (Ti-6Al-4V), and meets ASTM B348 specifications. Titanium is an elasto-plastic material without a well-defined yield plateau. Material properties of the titanium alloy bars are shown in Table D.3. A customized deformation pattern was created for the titanium to increase bond with the epoxy interface.

Table D.3 - NSM titanium material properties

Material	Bar Diameter (in.) [mm]	Bar Area ($in.^2$) [mm^2]	Grade (ksi) [MPa]	Actual f_y (ksi) [MPa]	Actual f_u (ksi) [MPa]	Elongation e_u (%)
Titanium	0.625 [15.9]	0.2975 [7.6]	N/A	145.4 [1002]	158.1 [1090]	11.2

D.2.4 Instrumentation

To collect data necessary for analysis, internal and external sensors were applied prior to testing. Data from all sensors were sampled at 5 Hz or 0.20 sec intervals.

D.2.4.1 Internal Sensor Array

Bondable foil strain gages were used for the internal sensor array. Because of the sensitivity of the strain gages, the output of the collected data was in units of microstrain, an amplified in/in (mm/mm) value.

The internal steel reinforcing bars were instrumented with strain gages prior to tying the reinforcing bar cage. Strain gages were at several locations along the length of the Mosier specimens. All specimens had identical strain gage locations to enable an accurate comparison between the control and strengthened specimens. A total of six strain gages were applied to the flexural tension steel. Four strain gages were applied to different reinforcing steel bars in the deck. One strain gage was applied to the #6 (19M) reinforcing steel bar at midspan. Five strain gages were applied to one leg of the transverse reinforcing steel at mid-height to measure the shear force at midspan. Strain gages were applied to the NSM titanium at coincident locations as the internal reinforcing steel and the end of the NSM titanium bars. Locations of the strain gages on the internal reinforcing steel and NSM titanium are shown in Figure D.15 through Figure D.17.

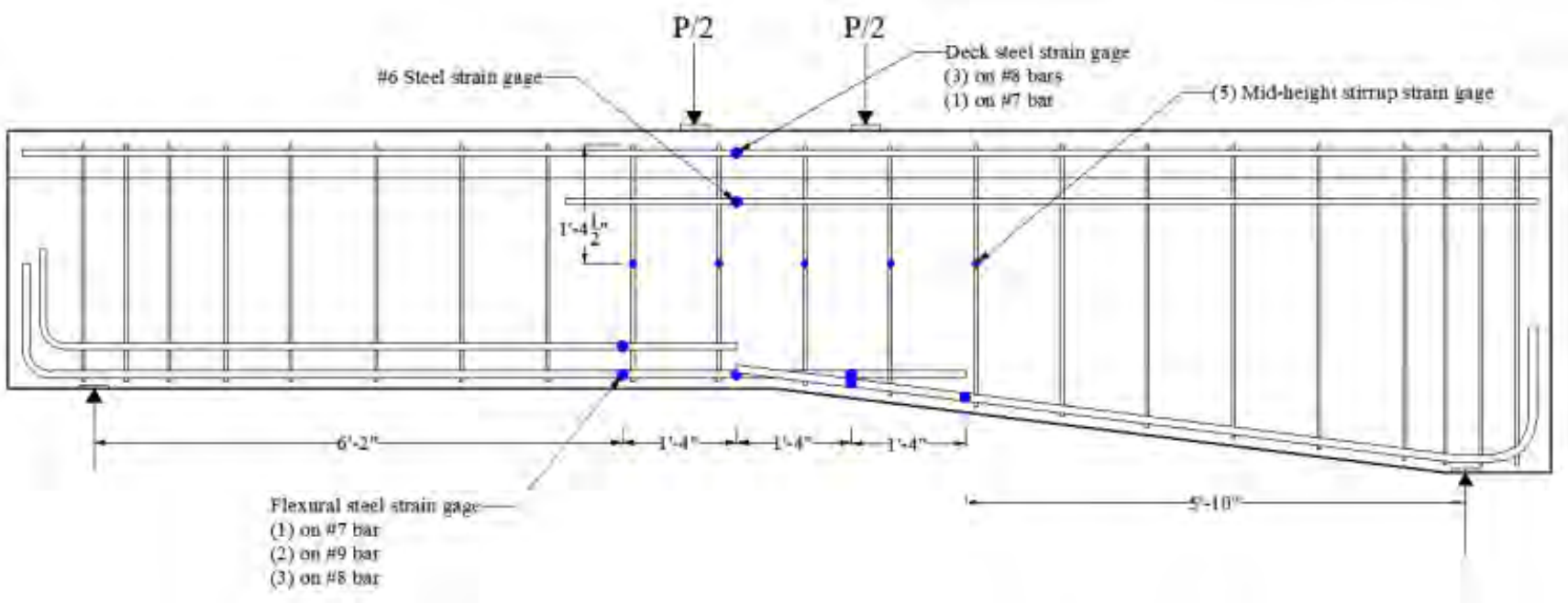

Figure D.15 - Internal sensor array of Mosier 1.

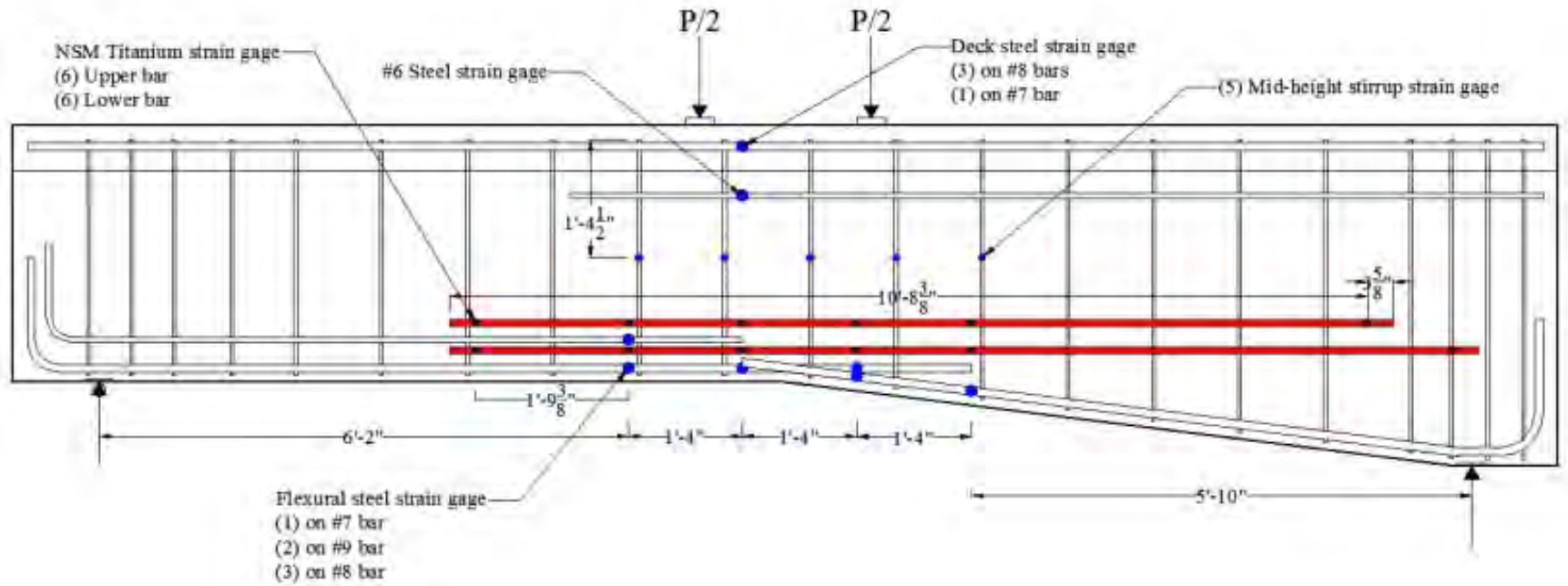

Figure D.16 - Internal sensor array of Mosier 2.

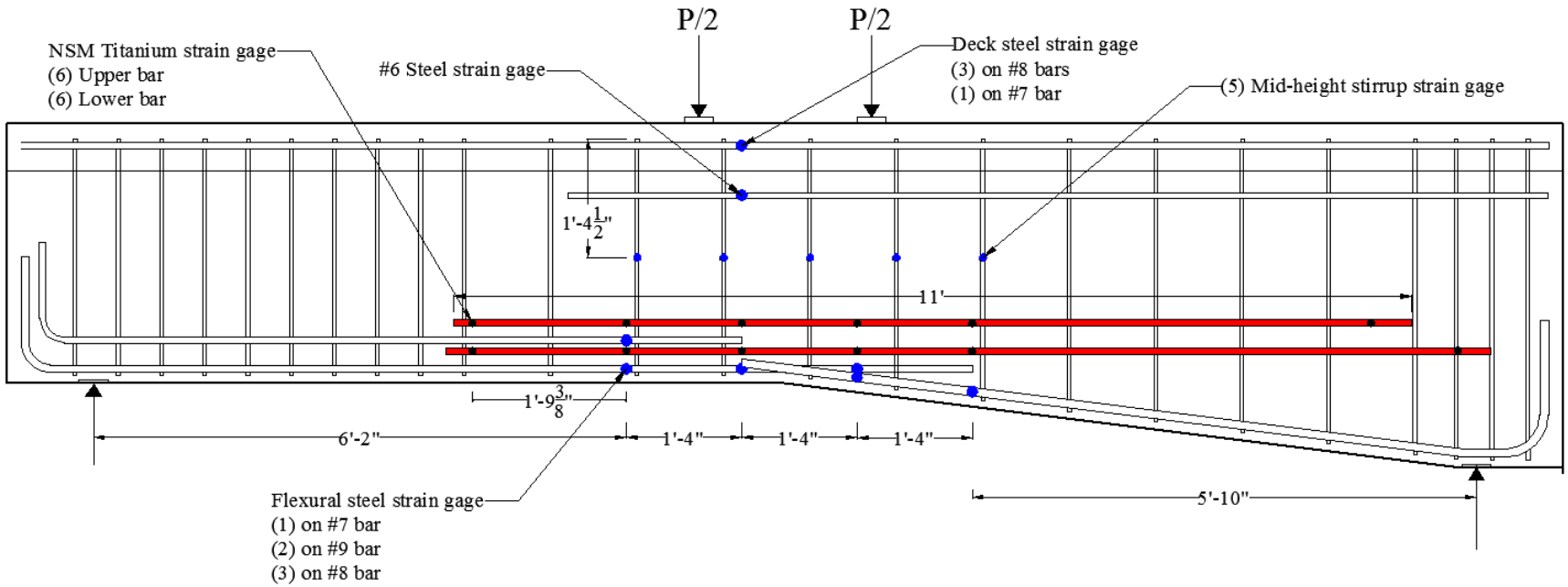

Figure D.17 - Internal sensor array of Mosier 3.

D.2.4.2 External Sensor Array

Three types of sensors were used to monitor the external response of the beam: string potentiometers, displacement sensors, and tilt sensors. All displacement sensors had units of inches and the tilt sensors measured in units of degrees.

The midspan displacement was monitored with two 10 in. (254 mm) stroke string potentiometers. Measuring displacement on each side of the web enabled the calculation of average midspan displacement. Each string potentiometer was attached to a steel dowel that was epoxied into the web.

Support settlements were measured with two 1.5 in. (38.1 mm) displacement sensors. The sensor was clamped to a metal stand and reacted off of an aluminum angle glued to the web of the beam. Measured North and South settlements were averaged and subtracted from the measured midspan displacement for the true midspan displacement.

The Mosier 1 specimen had a block-out around the end of the #8 (25M) bars. A 1 in. (25.4 mm) long stroke displacement sensor measured the slip of the #8 (25M) bar end relative to the concrete. Bar end slip was not measured for Mosier 2 or Mosier 3.

Tilt sensors were attached to one side of the web over each support. The sensors measured the rotation of each side of the specimen while loading.

Pairs of diagonal displacement sensors were used to measure crack width over regions of the beam. Each displacement sensor had a calibrated range of 1 in. (25.4 mm). The sensors were attached to small threaded rods epoxied in the web. The configuration of a typical diagonal displacement setup for the Mosier specimens is shown in Figure D.18.

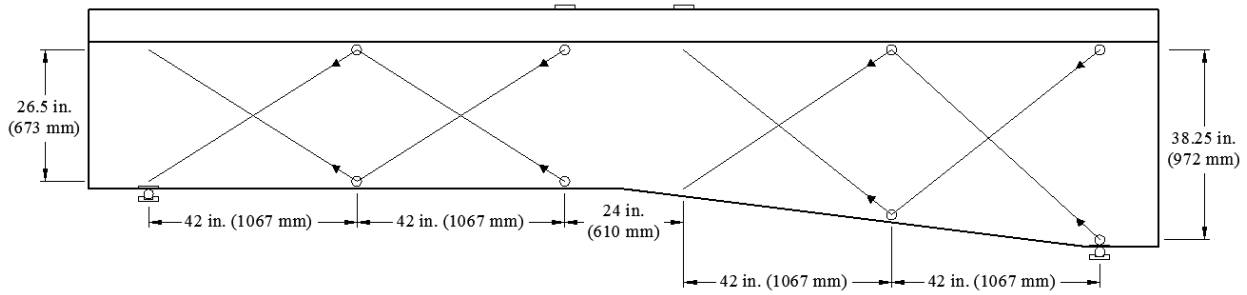

Figure D.18 - Typical specimen diagonal displacement sensor layout.

D.2.5 Test Protocols

All Mosier T-specimens were tested at the Oregon State University Structural Engineering Research Laboratory. The simply supported Mosier specimens had a span length of 18 ft (5.48 m) from centerline of supports. Due to the haunched geometry, a load cell was used under the South support as a spacer to level the flange. To simulate the dead load stresses in the Mosier Bridge, the specimen first required negative bending to be induced. A 100 kip (445 kN) hydraulic jack was placed under the soffit of the stem at midspan. An upward force of 34.5 kips (153 kN) was applied. To counteract this force, two steel tubes were placed on top of the deck and were tied into the strong floor with threaded rods shown in Figure. D.19a. Mosier 1 held the dead load forces for three days then was unloaded. Mosier 2 and Mosier 3 induced and held the

force for at least seven days while the NSM titanium epoxy was curing. The hydraulic jack was unloaded and removed before applying the positive bending loads.

To induce positive four-point bending, a reaction frame was anchored into the strong floor and held the servo-hydraulic load-controlled actuator. The actuator had a 500 kip (2224 kN) capacity and a 30 in. (762 mm) stroke. The actuator force was distributed through a spreader beam creating a 2 ft (610 mm) constant moment region at midspan shown in Figure D.19b. The specimen had a M/V ratio of approximately 4.1 ft (1.25 m), which corresponded closely to the computed M/V ratio in the bridge of 3.6 ft (1.10 m) All reaction points distributed the load from a 4 in. (101.6 mm) plate on a 2 in. (50.8 mm) diameter captive roller. Loading plates at midspan were leveled with a high strength grout. Prior to testing, the actuator was plumbed, and loading plates were shimmed if necessary.

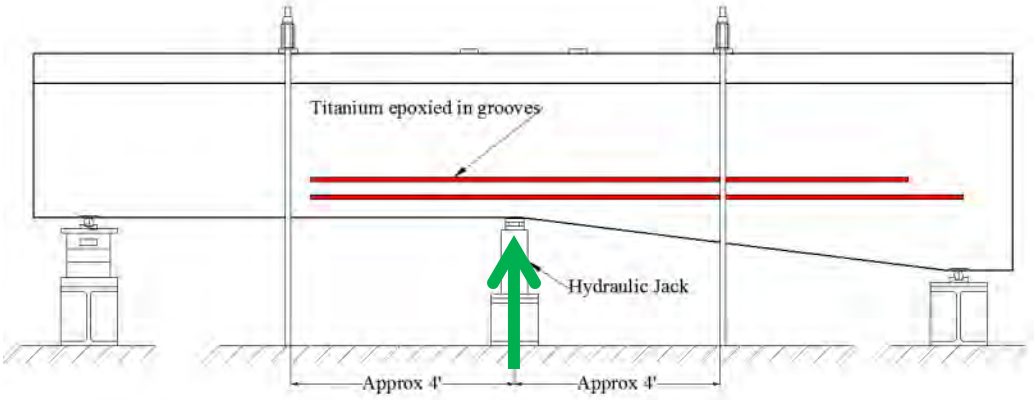

Figure D.19a - Configuration for inducing dead load stresses and NSM installation.

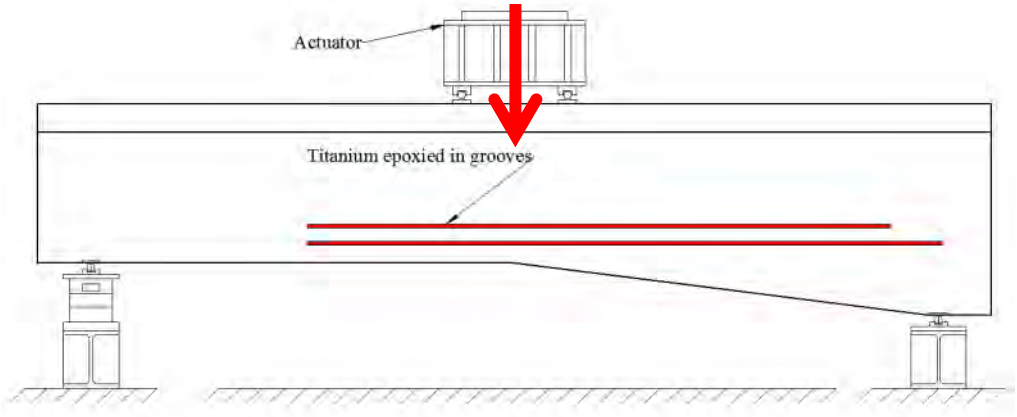

Figure D.19b - Configuration for applying actuator force representing live loads.

The positive bending load was applied at 10 kips (44 kN) increasing increments and unloaded to 5 kips (22.2 kN) between each cycle until failure in Mosier 1. The titanium strengthened specimens increased the applied load by increments of 25 kips (111 kN). The loading rate was pseudostatic at 0.15 kip/sec (0.67 kN/sec) without load reversals. After reaching each target load step, the load was reduced by at least 5 kips (22 kN) then held to minimize creep while cracks

were identified. If the specimen was close to failure the load cycle was extended until the maximum capacity was reached.

D.3 Experimental Results

This section describes the experimental results of the three Mosier specimens tested in this research program. The tested specimens were identified as Mosier 1, Mosier 2, and Mosier 3. The reported responses include the load deformation, anchorage slip, material strains, and strain along the section.

D.3.1 Overall Specimen Response

The NSM titanium strengthened Mosier specimens were tested to failure and achieved greater loads than the baseline specimen, Mosier 1. The NSM strengthened specimens experienced ductile flexural failures and displayed distributed cracking and signs of distress prior to failure. The applied load, shear, V_{APP}, dead load shear, $V_{DL,}$ total shear, $V_{EXP,}$ midspan displacement, and observed failure crack angle are reported in Table D.4. The reported midspan displacement corresponds to the peak load. The total shear is the applied shear from the actuator plus the dead load shear. Dead load shear was calculated from the weight of concrete acting across the failure plane.

Table D.4- Summary of specimen capacity and midspan displacement.

Specimen	Applied Load	Applied Shear (V_{APP})	DL Shear (V_{DL})	Total Shear (V_{EXP})	Midspan Disp.	Failure Crack Angle
	kips [MN]	kips [kN]	kips [kN]	kips [kN]	in. [cm]	deg.
Mosier 1	63.7 [0.283]	31.9 [141.6]	0.27 [1.2]	31.1 [142.8]	0.258 [6.55]	68
Mosier 2	138.4 [0.615]	69.2 [307.8]	0 [0]	69.2 [307.8]	1.02 [25.9]	90
Mosier 3	131.5 [0.585]	65.8 [292.5]	0 [0]	65.8 [292.5]	1.01 [25.7]	90

D.3.1.1 Load Deformation Response

The load and displacement response describes the overall behavior of the specimens. Load deformation responses for the NSM-retrofitted and baseline Mosier specimens are shown in Figure D.20. Mosier 1 was loaded in 10 kip (44.5 kN) increments, then unloaded, and then proceeded to the next load step until eventual failure. Mosier 2 and Mosier 3, the NSM titanium specimens, had a larger predicted capacity and was loaded in 25 kip (111 kN) increments, unloaded to 5 kips (22.2 kN), and then proceeded to the next load step until failure.

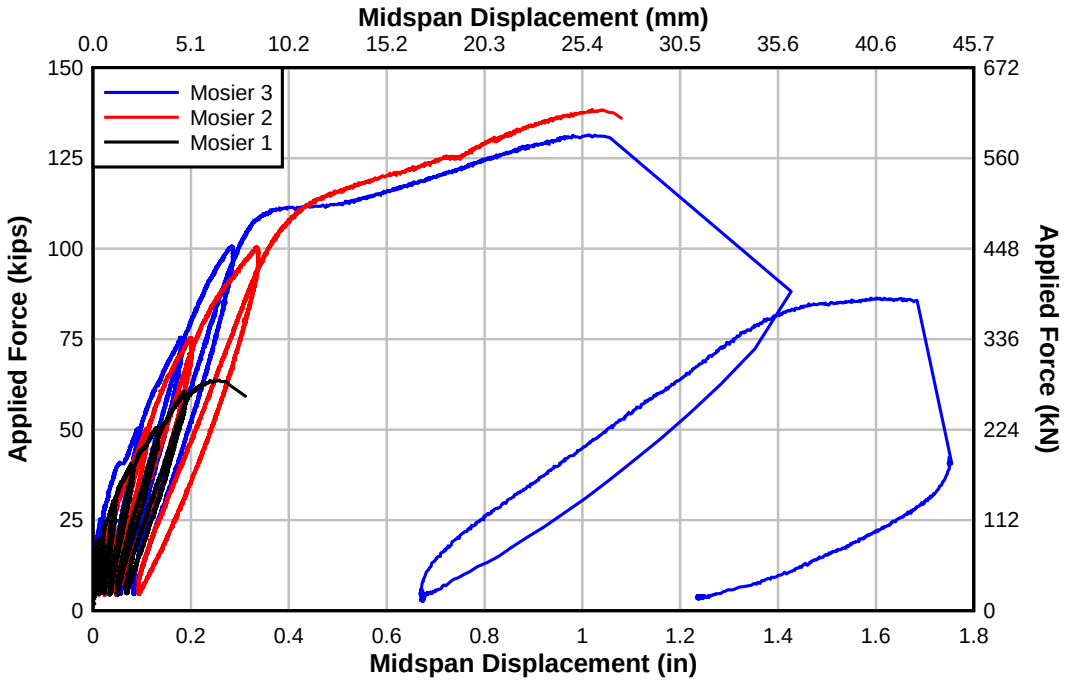

Figure D.20 - Mosier specimens applied load and measured displacement response.

Mosier 2 and Mosier 3 specimens increased the baseline specimen load capacity by 74.7 kip (332 kN) and 67.8 kip (302 kN) respectively. The deflection of the strengthened specimens increased by 0.762 in. (19.3 mm) and 0.752 in. (19.1 mm) compared to the baseline for Mosier 2 and Mosier 3 respectively. Mosier 2 had a slightly lower stiffness than Mosier 3 because initial cracking of the concrete and slip of the cutoff reinforcing steel bars occurred prior to testing. The load was being carried by the NSM titanium that had a much lower modulus of elasticity. Mosier 3 maintained a composite section which lead to a stiffer response until the specimen became inelastic. Once inelastic, at approximately 109 kips (484 kN), Mosier 3 experienced a significant slip of the internal reinforcing which damaged the bond of the NSM titanium alloy bars. The damaged bond of the NSM titanium bars contributed to the slight decrease in ultimate capacity compared to Mosier 2.

Mosier 3 exhibited a significant amount of reserve capacity after failure. This reserve capacity is seen as the last load cycle upon which Mosier 3 achieved a load of 88 kips (391 kN). The reserve capacity indicates that the NSM titanium alloy bars with mechanical anchorages could sustain loads above the factored demands after bond rupture along the length that occurred at peak load.

D.3.1.2 Crack Propagation

Concrete crack initiation and propagation was monitored throughout the test. After each load cycle, the load was decreased and then held to minimize creep effects. During this time, the specimens were inspected and cracks were measured and highlighted. Digital pictures were taken at each load step to record the cracked condition. The crack patterns at failure are shown in for each specimen in Figure D.21. Digital photographs at failure are shown in Figures D.22 through D.24.

Mosier 1

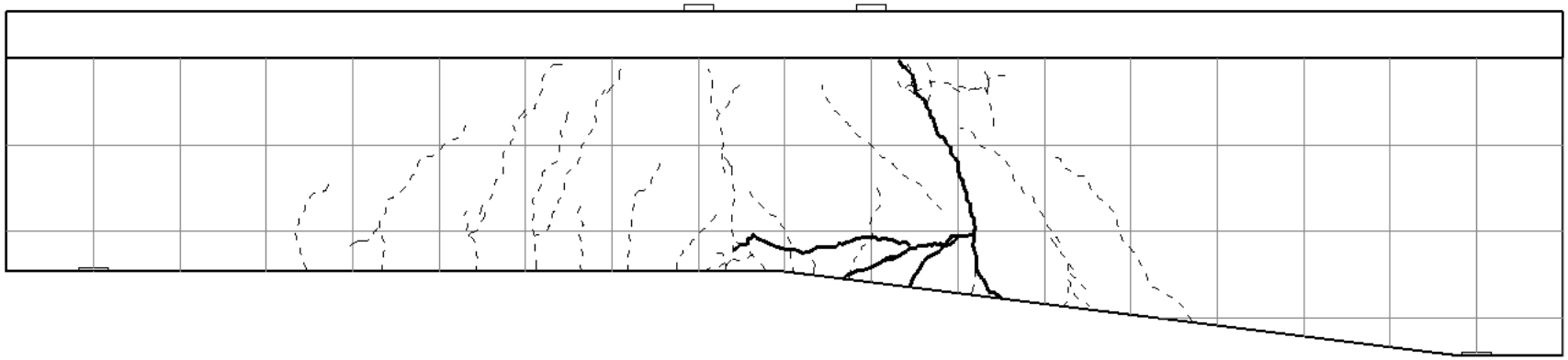

Mosier 2

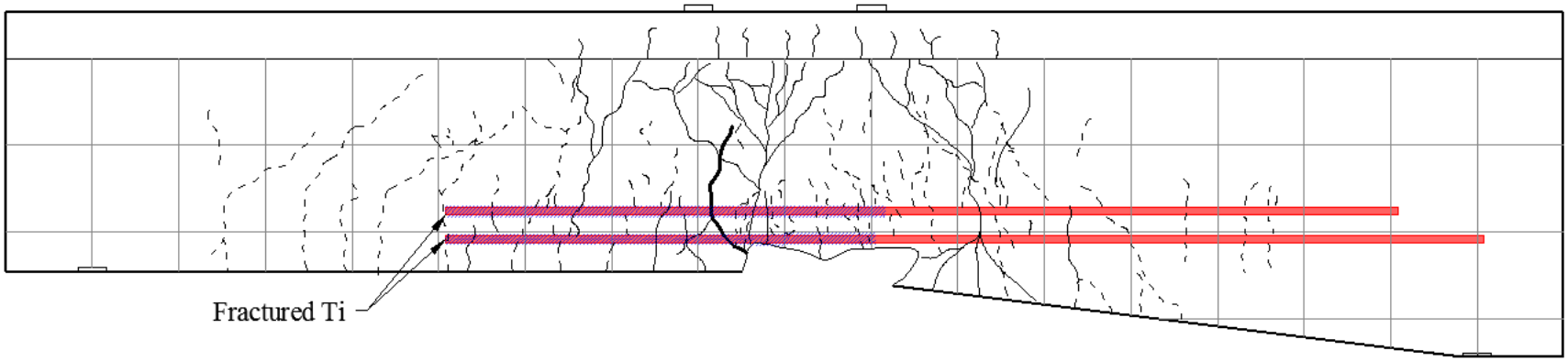

Mosier 3

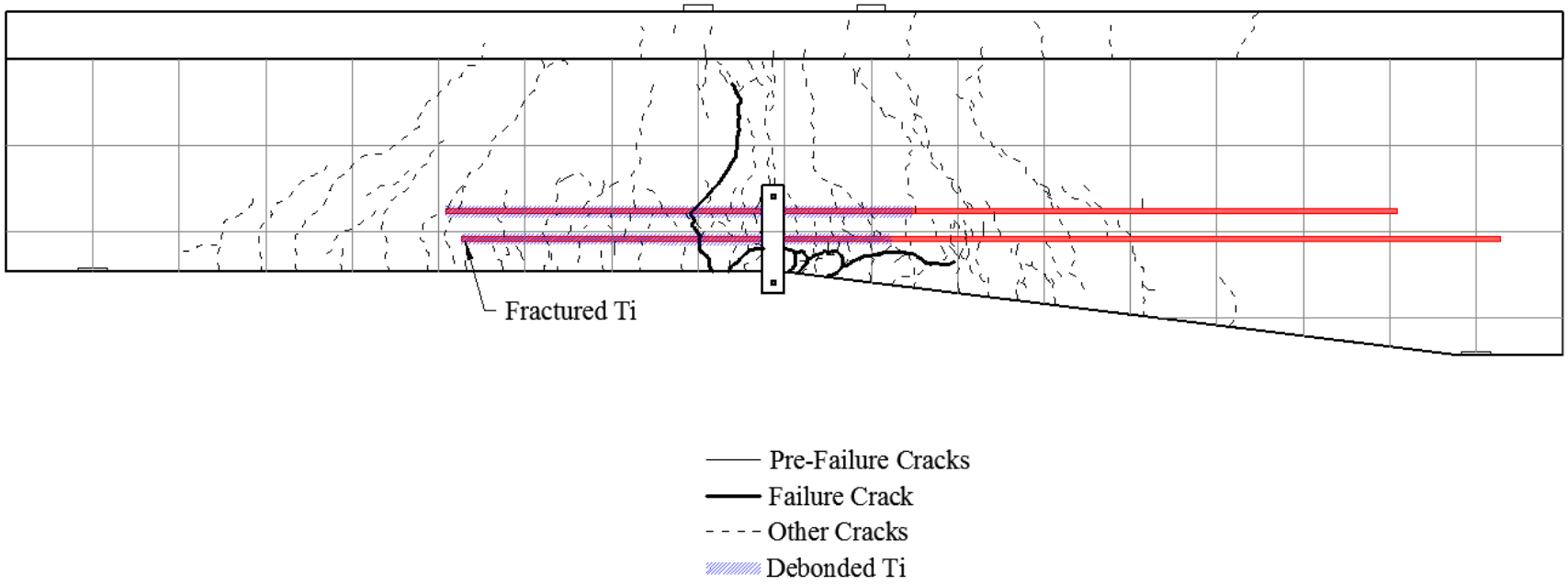

Figure D.21- Cracks observed on Mosier specimens.

Figure D.22 - Mosier 1 failure photograph.

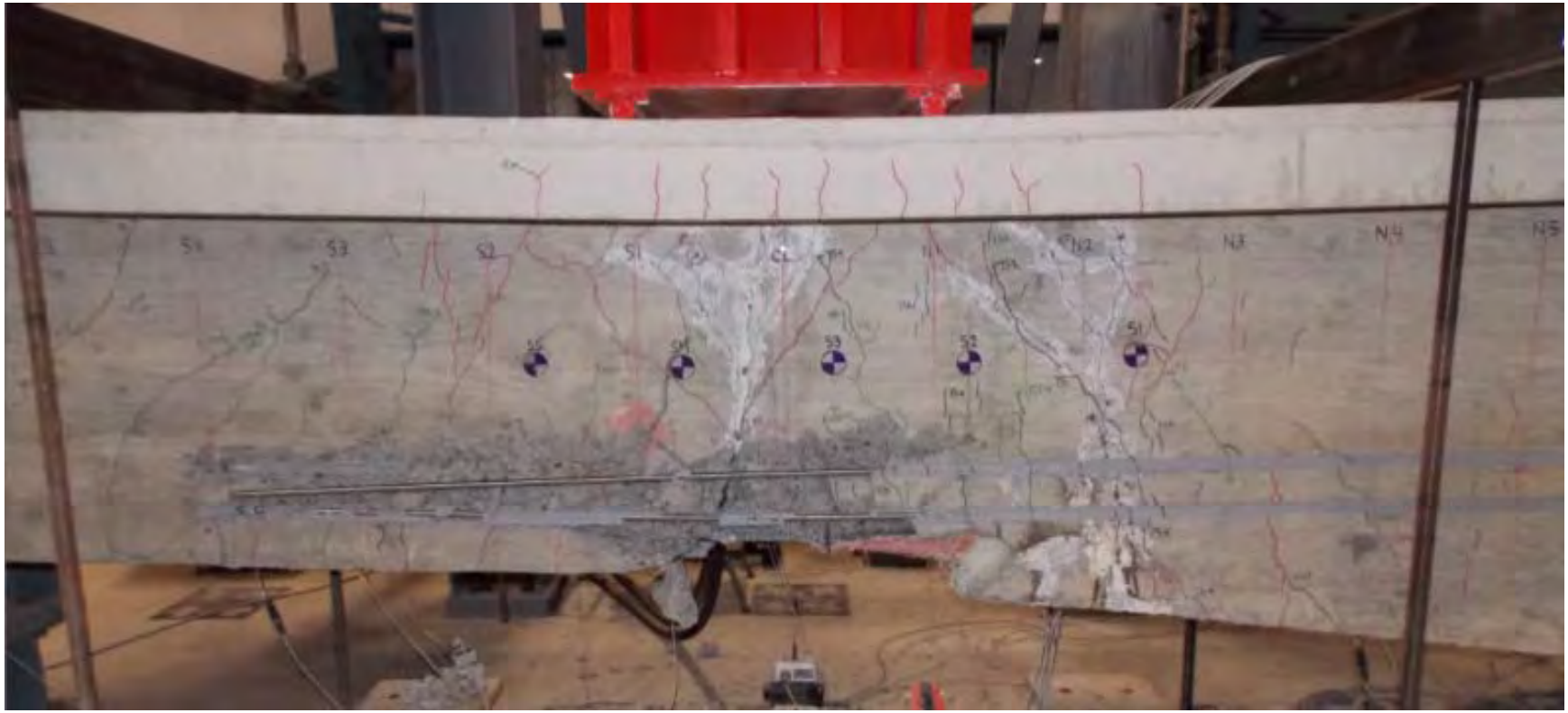

Figure D.23 - Mosier 2 failure photograph.

Figure D.24 - Mosier 3 failure photograph.

.

The Mosier 1 specimen failed in flexure and exhibited similar cracking patterns to the cracks observed in the Mosier Bridge. Mosier 2 and Mosier 3 specimens failed in flexure after debonding of the NSM titanium alloy bars. The debonding, or delamination, of the NSM titanium alloy bars initiated at midspan and propagated to the embedded NSM hook ends. After delamination of the NSM titanium bars, three out of the four titanium hooks fractured on the South end of Mosier 2. During failure of Mosier 3, all NSM titanium hooks remained intact at initial failure. After reloading and achieving the reserve capacity, one hook fractured and one hook was dislodged on the south end of Mosier 3. Chevron cracks, typical of anchorage failures, appeared near failure in all specimens. The chevron cracks were constrained by the NSM titanium. The NSM titanium strengthened specimens experienced distributed cracking over the constant moment region to the end of the NSM titanium bars in the south end of the specimen. Longitudinal cracks along the epoxy-concrete interface coincided with the abrupt debonding failure of specimens Mosier 2 and Mosier 3. The widespread extent of macro cracking in the concrete and around the epoxy provided visual indication of distress prior to failure. An example close-up view of the cracking around the NSM-titanium alloy bars prior to bond rupture is shown in Figure D.25.

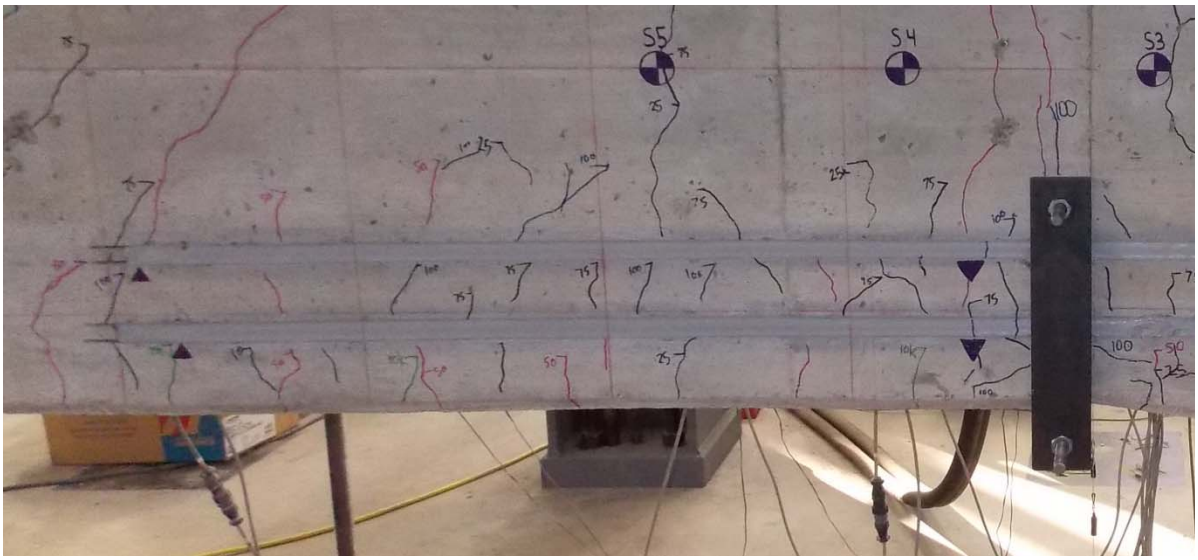

Figure D.25 – Close-up view of cracking around the NSM-titanium alloy bars prior to bond rupture.

D.3.1.3 Anchorage Slip Response

As the applied load increased, the internal reinforcing steel bars slipped regardless of the failure mode or location. Cutoff reinforcing bar slip sensors installed near the block-out on the #8 (25M) bars measured the reinforcing bar slip with respect to load in Figure D.26.

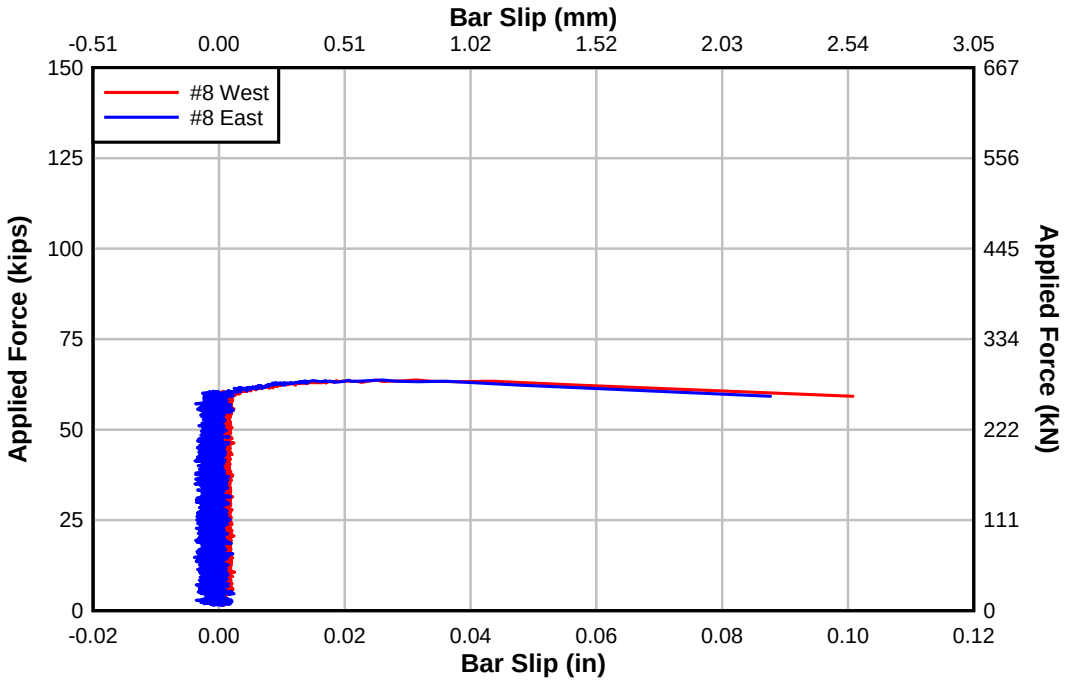

Figure D.26 – Slip response of #8 Steel reinforcing bars in Mosier 1.

The East and West #8 (25M) steel reinforcing bars had similar rates of slip throughout the test. Significant slips did not occur in the #8 (25M) steel reinforcing bar until near failure loads. Near the failure load, chevron cracking developed around the #8 (25M) bar.

Slip of the #8 (25M) steel reinforcing bar was not recorded in the Mosier 2 and Mosier 3 specimens so as to not disrupt the bond along the NSM bars. However, apparent slip of the #9 (29M) steel reinforcing bars is shown Figure D.27 for Mosier 2 and Figure D.28 for Mosier 3.

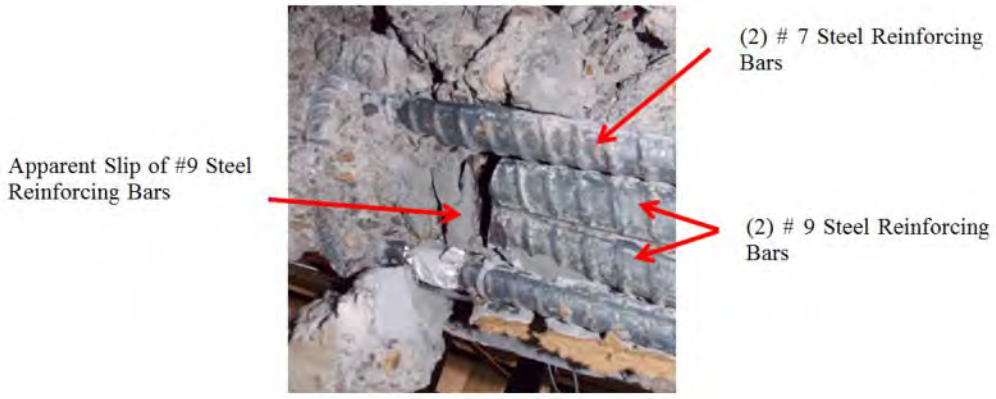

Figure D.27 - Apparent slip of # 9 Steel Reinforcing Bars in Mosier 2.

Figure D.28 - Apparent slip of #9 Steel Reinforcing Bars in Mosier 3.

The digital images also illustrate the lack of concrete cover and reinforcing steel congestion surrounding the #8 (25M) and #9 (29M) steel reinforcing bars that is contained in the original design.

D.3.1.4 Material Strains

Top, bottom, and NSM bar strains were plotted at each instrumented cross section. This comparison illustrates the interaction between the NSM bar and developing cutoff bar. The section labels start from the southernmost strain gage location on the NSM titanium bar. Therefore, section 1 on Mosier 1 does not exist. A guide for the sections is shown in Figure D.29. Strains for materials at cross sections along the length of the specimen are found for Mosier 1 in Figure D.30 through Figure D.33.

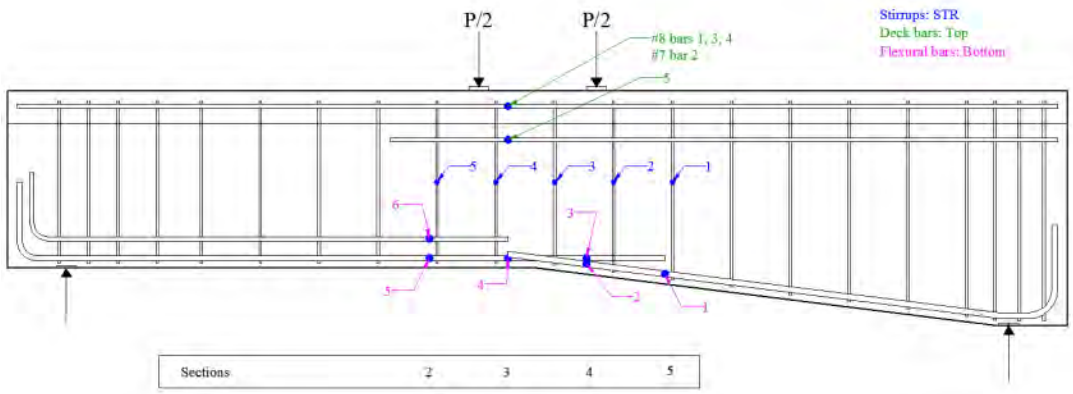

Figure D.29 - Strain gage configuration for Mosier 1.

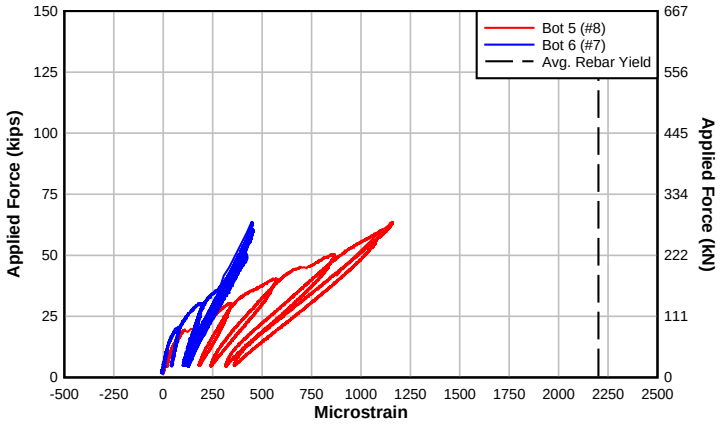

Figure D.30 - Mosier 1 Section 2.

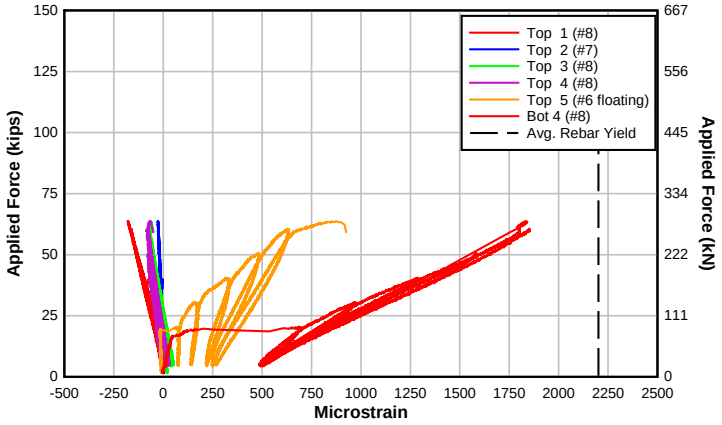

Figure D.31 - Mosier 1 Section 3.

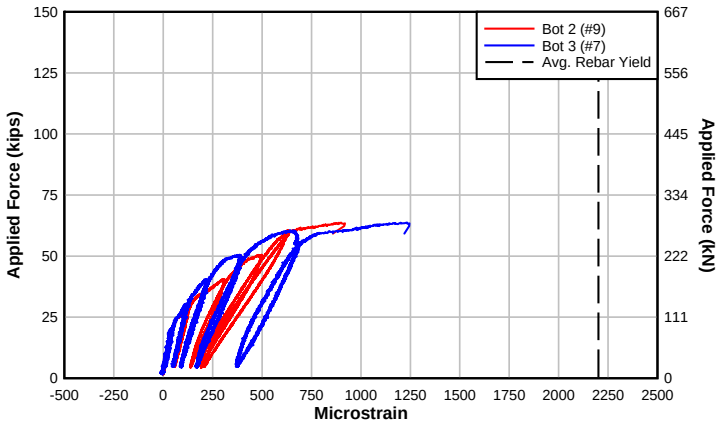

Figure D.32 - Mosier 1 Section 4.

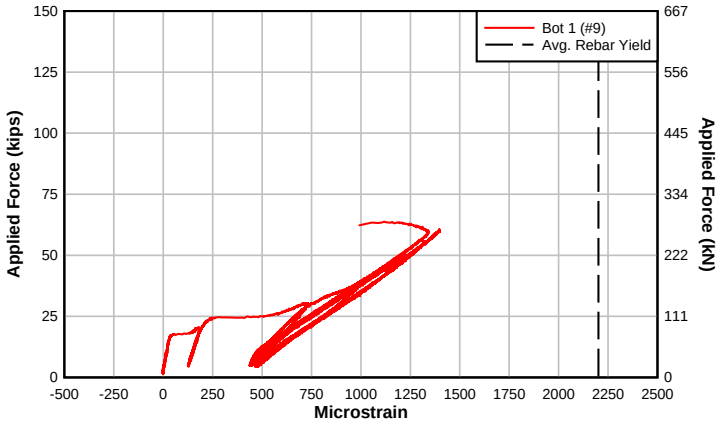

Figure D.33 - Mosier 1 Section 5.

A guide for the instrumented sections in Mosier 2 is shown in Figure D.34.Sectional strains for Mosier 2 are shown in Figure D.35 through Figure D.40. Note that the yield strain for the titanium alloy bars is 9000 με and the strain gages applied to the bars are only rated to provide strains to 3000 με.

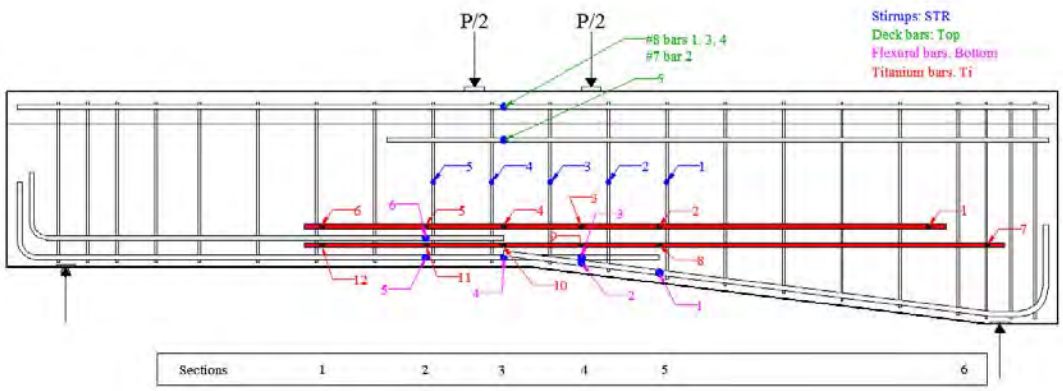

Figure D.34 - Strain gage configuration for Mosier 2 and Mosier 3.

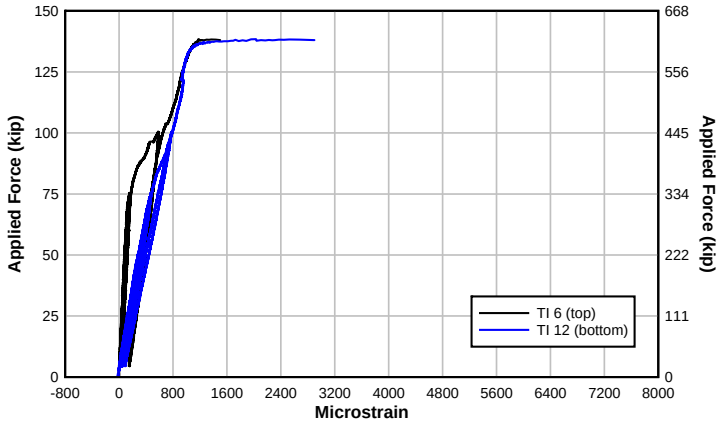

Figure D.35 - Mosier 2 Section 1 (Note: yield strain for titanium is 9000 με).

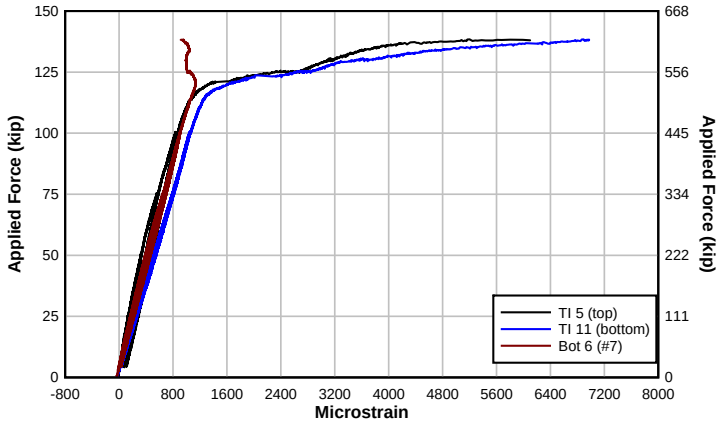

Figure D.36 - Mosier 2 Section 2.

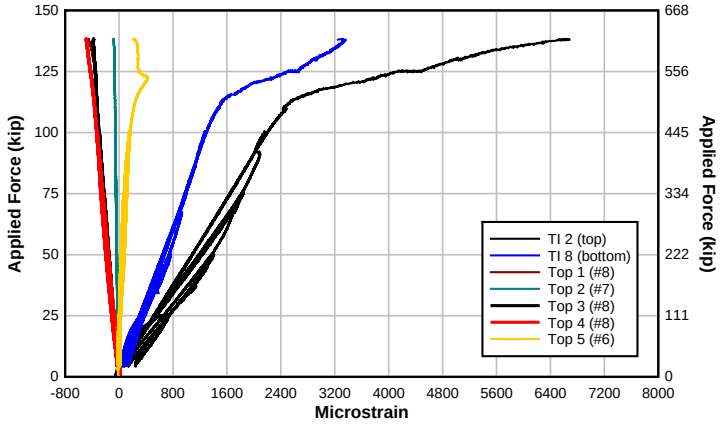

Figure D.37 - Mosier 2 Section 3.

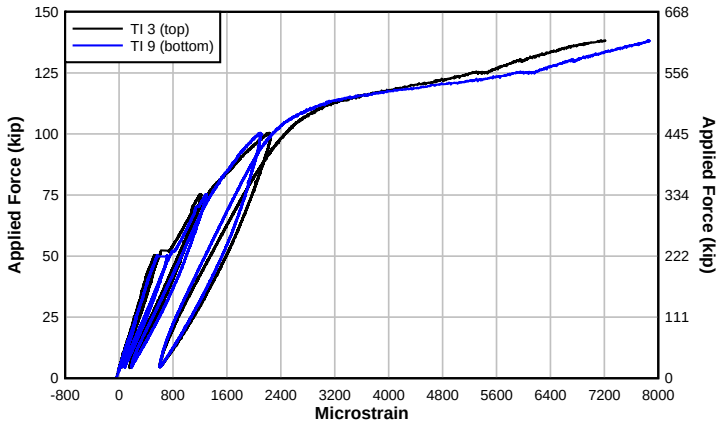

Figure D.38 - Mosier 2 Section 4.

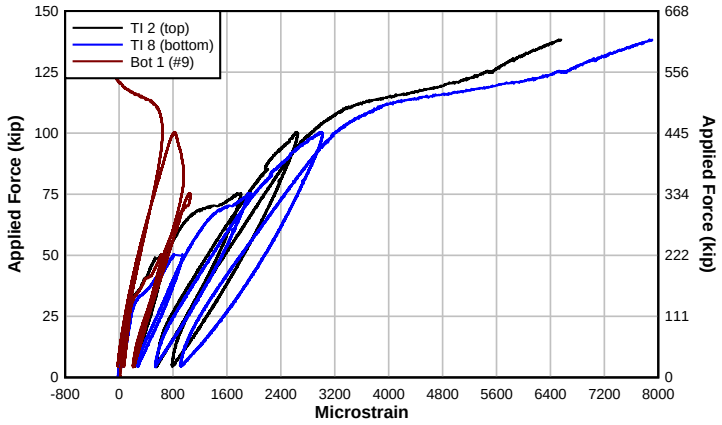

Figure D.39 - Mosier 2 Section 5.

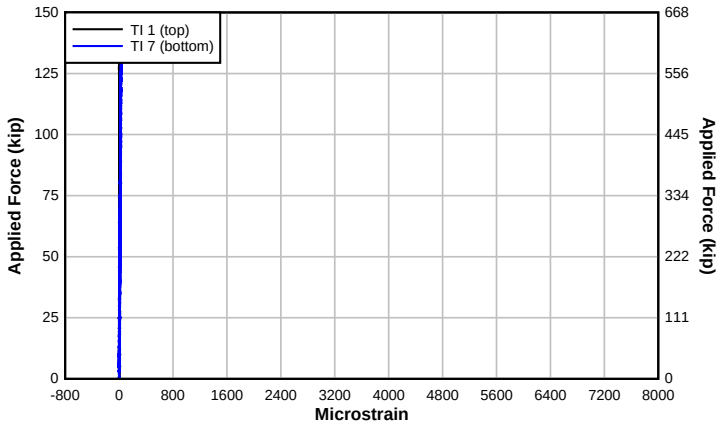

Figure D.40 - Mosier 2 Section 6.

Strains at each section are shown for Mosier 3 in Figure D.41 through Figure D.46.

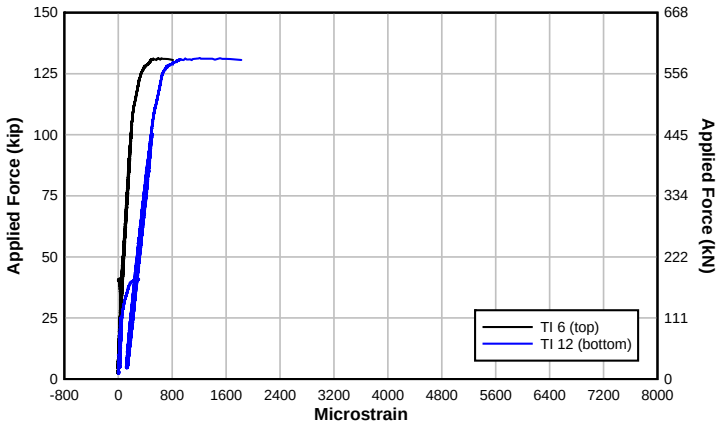

Figure D.41 - Mosier 3 Section 1.

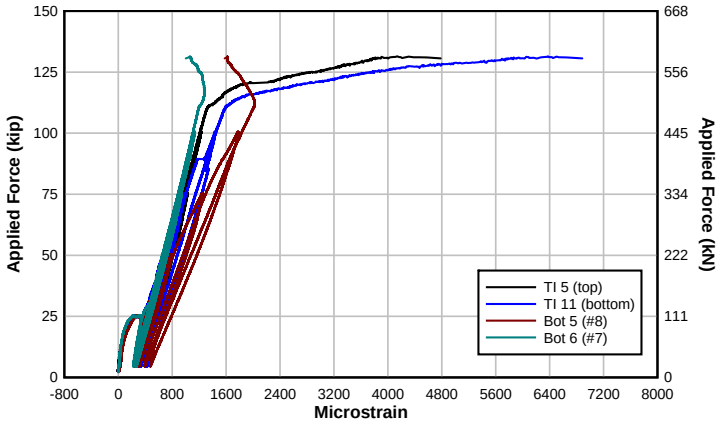

Figure D.42 - Mosier 3 Section 2.

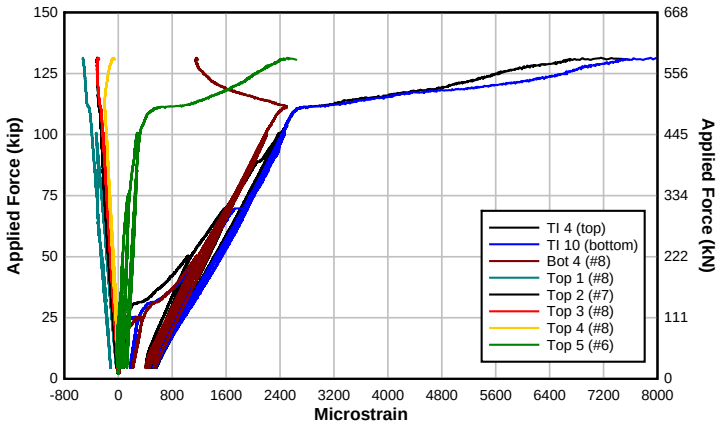

Figure D.43 - Mosier 3 Section 3.

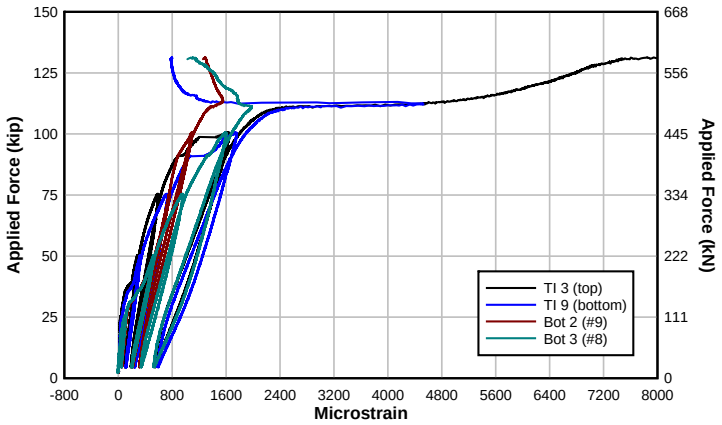

Figure D.44 - Mosier 3 Section 4.

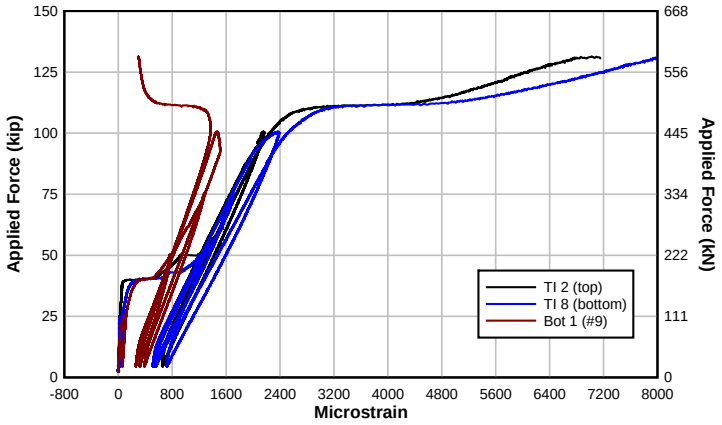

Figure D.45 - Mosier 3 Section 5.

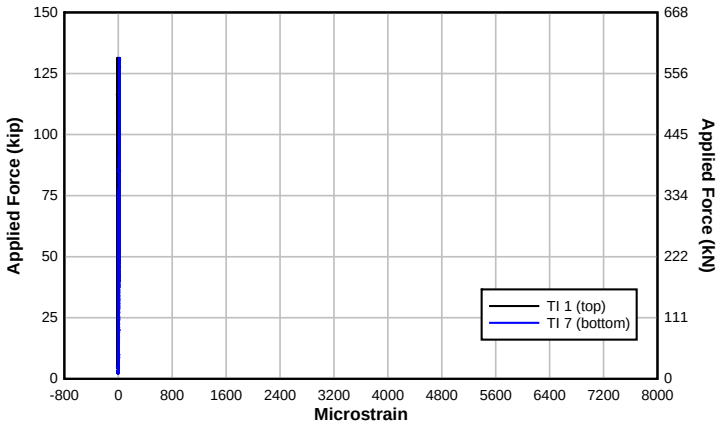

Figure D.46 - Mosier 3 Section 6.

Strains in the NSM titanium were negligible at the North end hook locations. The south end of the NSM titanium hooks had very linear strain until failure. Strain reversal in the #9 (29M) steel reinforcing bars indicated bar slip in the NSM titanium specimens. The strain reversal in the #7 (25M) was due to bar slip and neighboring bar slip of the #9 (29M) steel reinforcing bar.

Midheight stirrup strains are shown in Figure D.47 through Figure D.49 for the Mosier specimens. The NSM titanium strengthened specimens exhibit much larger strains that Mosier 1 due to the increased flexural strength provided by the NSM titanium bars. Yield strain for the stirrups was around 1731 microstrain, which means that none of the stirrups reached yield.

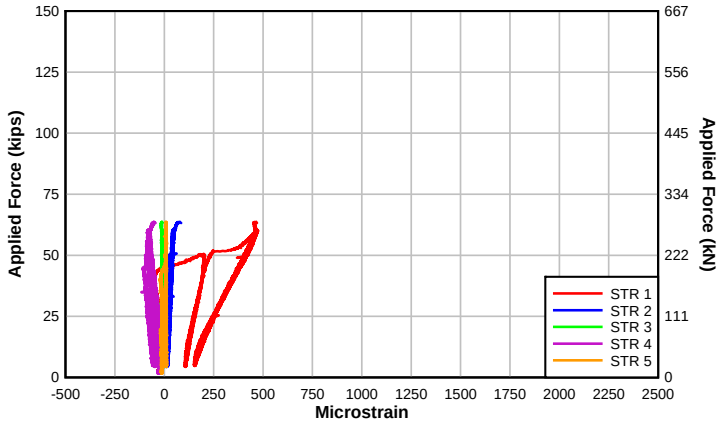

Figure D.47 - Mosier 1 Stirrup strains.

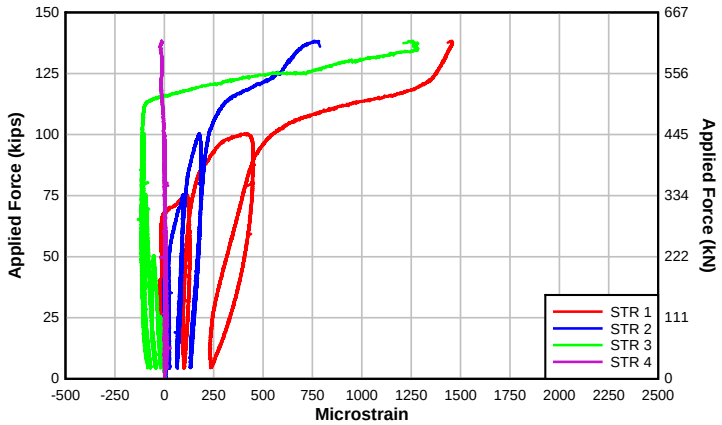

Figure D.48 - Mosier 2 Stirrup strains.

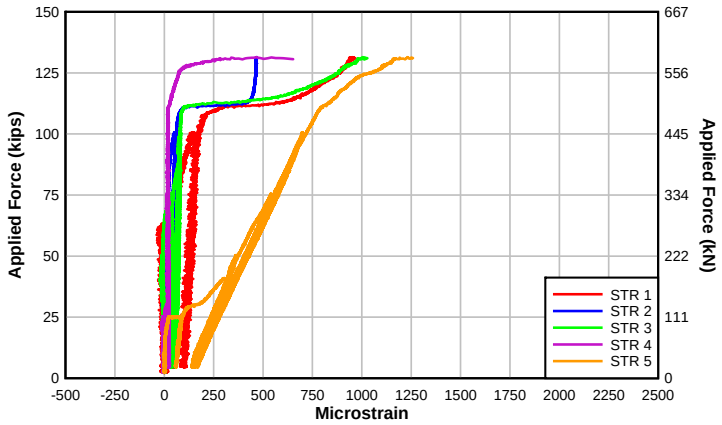

Figure D.49 - Mosier 3 Stirrup strains.

D.4 Design and Analytical Predictions

Analysis of the Mosier Bridge produced a factored moment demand at the critical section of 219 kip-ft (297 kN-m) which was 46 kip-ft (63 kN-m) above the AASHTO-LRFD computed design moment capacity of the section. Considering the observed distress, it signified the need for

strengthening. The design intent of the Mosier specimens was to strengthen the baseline specimen, Mosier 1, to a level above the required design strength, M_u. The moment capacity of Mosier 1 was computed using AASHTO-LRFD and Response 2000 and is shown relative to the experimentally observed response in Figure D.50. In the R2K analysis, the partial contribution of the poorly detailed reinforcing steel at midspan was included based on the available development length relative to the computed development length using ACI 318 complex approach. The R2K predicted flexural capacity of Mosier 1 was within 3 kip-ft (4 kN-m) of the observed value and shows that the partially developed steel should be included in the analysis.

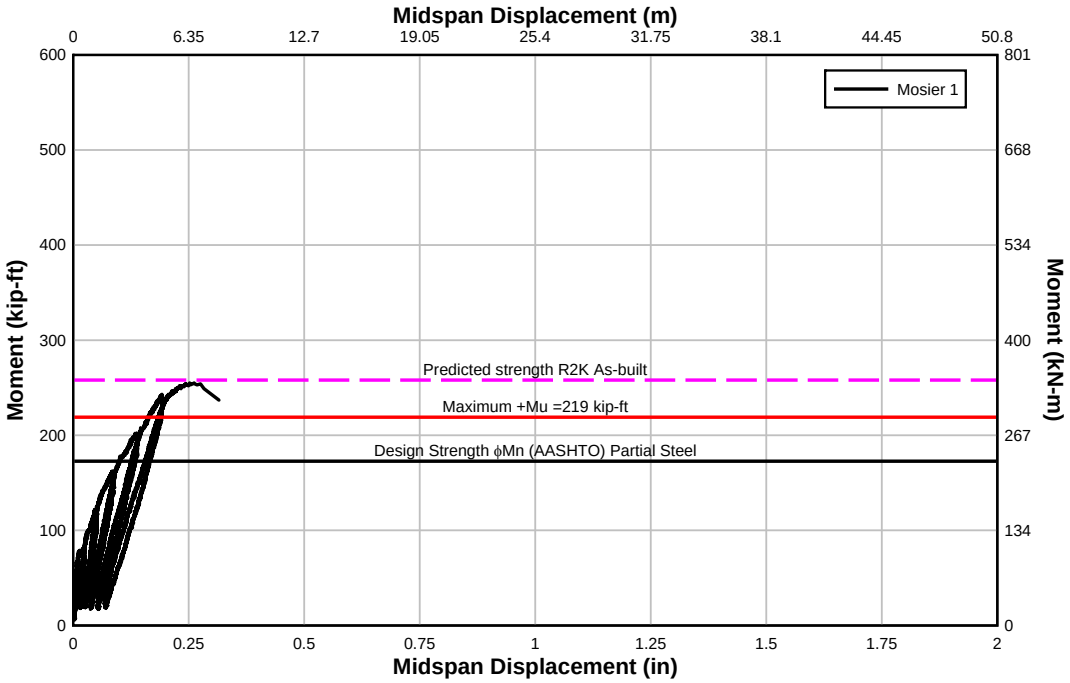

Figure D.50 - Mosier 1 predicted and experimental capacities.

The strengths of the NSM strengthened specimens were also predicted using AASHTO and R2K and are shown in Figure D.51 relative to the experimental results. The solid lines show the AASHTO predictions with and without the partial contribution of reinforcing steel at midspan. The dashed lines represent the R2K flexural capacities with and without partial contribution of reinforcing steel at midspan. As seen in the figure, improved predictions for member strength were achieved when the partially developed internal steel was used in the analysis.

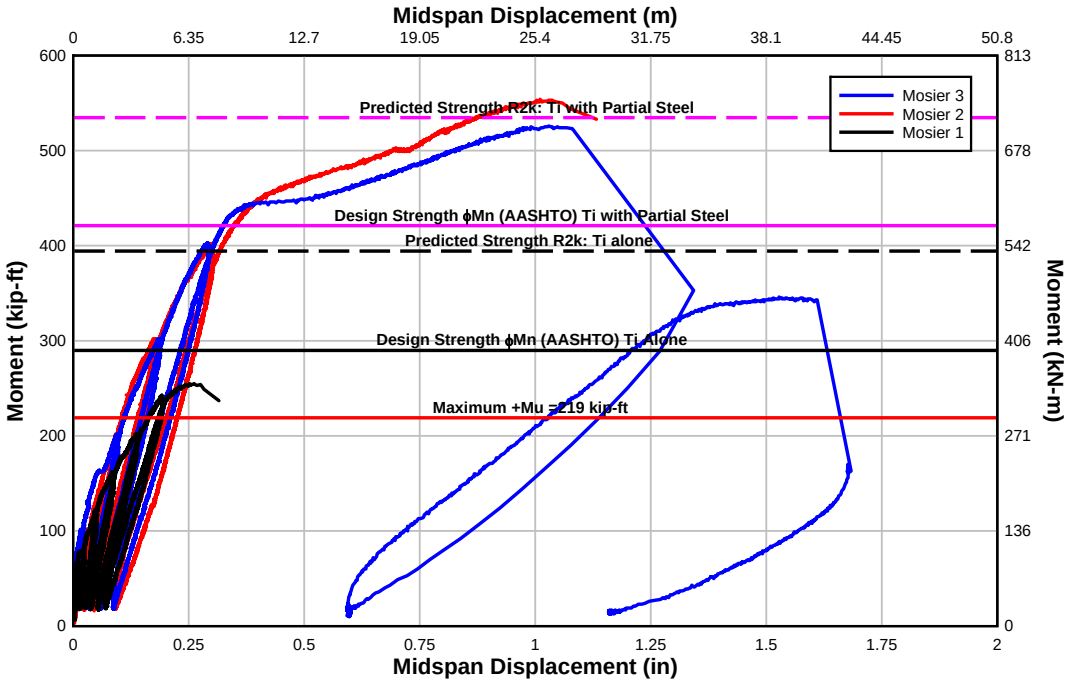

Figure D.51 - Mosier specimens predicted and experimental capacities.

The most conservative prediction of the NSM strengthened member capacity (AASHTO design moment capacity relying only on the NSM titanium and assuming the internal steel provides no resistance) exceeded the factored moment demand at the critical section. The analysis results showed that inclusion of the partially embedded or developed internal reinforcing steel at midspan provided better prediction of member strength. R2K reasonably predicted the capacity of the NSM strengthened specimens assuming fully anchored NSM titanium alloy bars.

D.5 Discussion of Results

Experimental tests of girder specimens proportioned based on the Mosier Bridge were performed. The control specimen exhibited cracking similar to that observed in the Mosier Bridge, confirming that the model fairly represented the field conditions. The control specimen, Mosier 1, did not meet AASHTO-LRFD requirements for moment capacity at the poorly detailed section located at the end of the haunched section. The R2K predicted capacity of Mosier 1 was in very good agreement with the experimental results.

The NSM titanium strengthening of Mosier 2 and Mosier 3 used four titanium alloy bars epoxied into a groove cut into the concrete cover of the specimen. The bars were terminated with 2 in. (51 mm) diameter radius, 90° hooks. The lengths of the hooks were determined by the width of the web in Mosier 2 and Mosier 3. Mosier 3 offset the terminations of the south end NSM titanium bars to smooth the transition of the bars. Mosier 3 also confined the NSM titanium material at midspan with a steel plate attached through the web.

The NSM titanium strengthened specimen, Mosier 2, was repaired after initially failing the anchorages of the internal reinforcing steel bars at midspan. This specimen achieved a slightly higher capacity than the Mosier 3 specimen which had the internal reinforcing steel fully intact.

Since the ends of the reinforcing steel were not confined at midspan, cracking and dilatation of the concrete upon slip of the internal steel reinforcing bars disturbed the NSM-epoxy concrete bond in Mosier 3 compared with Mosier 2. Mosier 2 and Mosier 3 exhibited similar midspan moment and displacement curves, but upon slip of the internal steel bars, increased deformations were observed in Mosier 3. Both specimens achieved similar load levels. Chevron cracks were observed over the cutoff reinforcing steel bars prior to failure. The titanium alloy bars helped delay the cutoff bar slip and produced a large increase in the ductility (more than quadrupled) and capacity (more than doubled) of the as-built specimen.

All specimen strengths were reasonably predicted by the R2K sectional analysis assuming fully anchored NSM titanium alloy bars and including partially developed internal reinforcing bars at the section. The strength was conservatively predicted using AASHTO-LRFD assuming the NSM titanium alloy bars were at the prescribed yield stress.